REPORT DOCUMENTATION PAGE

Form Approved
OMB No. 0704-0188

Public reporting burden for this collection of information is estimated to average 1 hour per response, including the time for reviewing instructions, searching existing data sources, gathering and maintaining the data needed, and completing and reviewing this collection of information. Send comments regarding this burden estimate or any other aspect of this collection of information, including suggestions for reducing this burden to Department of Defense, Washington Headquarters Services, Directorate for Information Operations and Reports (0704-0188), 1215 Jefferson Davis Highway, Suite 1204, Arlington, VA 22202-4302. Respondents should be aware that notwithstanding any other provision of law, no person shall be subject to any penalty for failing to comply with a collection of information if it does not display a currently valid OMB control number. **PLEASE DO NOT RETURN YOUR FORM TO THE ABOVE ADDRESS.**

1. REPORT DATE *(DD-MM-YYYY)*
20-07-2016

2. REPORT TYPE
Final Technical Report

3. DATES COVERED *(From - To)*
01 Feb 2010 to 30 April 2016

4. TITLE AND SUBTITLE
Refined Source Terms in WAVEWATCH III with Wave Breaking and Sea Spray Forecasts

5a. CONTRACT NUMBER

5b. GRANT NUMBER
N00014-10-1-0390

5c. PROGRAM ELEMENT NUMBER

6. AUTHOR(S)
Banner, Michael, L.
Morison, Russel, P.
Fairall, Christopher, W.

5d. PROJECT NUMBER

5e. TASK NUMBER

5f. WORK UNIT NUMBER

7. PERFORMING ORGANIZATION NAME(S) AND ADDRESS(ES)
UNIVERSITY OF NEW SOUTH WALES
UNSW Grants Management Office
Level 3, South Wing, Rupert Myers Building
SYDNEY NSW 2052 AUSTRALIA

8. PERFORMING ORGANIZATION REPORT NUMBER

9. SPONSORING / MONITORING AGENCY NAME(S) AND ADDRESS(ES)
Office of Naval Research
495 Summer Street
Suite 627
Boston, MA 02210-2109

10. SPONSOR/MONITOR'S ACRONYM(S)

11. SPONSOR/MONITOR'S REPORT NUMBER(S)

12. DISTRIBUTION / AVAILABILITY STATEMENT
APPROVED FOR PUBLIC RELEASE

13. SUPPLEMENTARY NOTES

14. ABSTRACT

15. SUBJECT TERMS

16. SECURITY CLASSIFICATION OF:			**17. LIMITATION OF ABSTRACT**	**18. NUMBER OF PAGES**	**19a. NAME OF RESPONSIBLE PERSON**
					Dr. Michael L. Banner
a. REPORT	**b. ABSTRACT**	**c. THIS PAGE**			**19b. TELEPHONE NUMBER** *(include area code)*
					+612419237177

Standard Form 298 (Rev. 8-98)
Prescribed by ANSI Std. Z39.18

FINAL REPORT

Refined Source Terms in WaveWatch III with Wave Breaking and Sea Spray Forecasts

Michael L. Banner
School of Mathematics and Statistics, The University of New South Wales, Sydney 2052, Australia
Tel: (+61-2) 9385-7064 fax: (+61-2) 9385-7123 email: m.banner@unsw.edu.au

Russel P. Morison
School of Mathematics and Statistics, The University of New South Wales, Sydney 2052, Australia
Tel: (+61-2) 9385-7064 fax: (+61-2) 9385-7123 email: r.morison@unsw.edu.au

Christopher W. Fairall
NOAA/ERSL, 325 Broadway, Boulder, Co 80305-3337, USA
Tel: 303 497 3253 email: chris.fairall@noaa.gov

Award No. N00014-10-1-0390

Submission Date: 5 August, 2016

Executive Summary

As marine winds strengthen, wave breaking becomes increasingly widespread. This has important consequences, both for offshore operations and geophysically, yet wave breaking is not included in present marine forecasts. This project addressed the challenge of incorporating wave breaking physics into coupled sea state marine weather forecasting models. The aim was to add accurate wave breaking and sea spray forecasts to the standard suite of forecast sea state variables, for sea state conditions ranging from light to very severe.

Our approach required a combination of observational and modeling efforts. We synthesized results from our field data analyses into accurate parameterizations for wave breaking occurrence and strength. We also needed to modify the wind input source term for compatibility with the other source terms and physical constraints. These refinements were incorporated in the dissipation and wind input source terms in the spectral wave evolution models used to generate forecasts.

Model development focused on wide spectral bandwidth computations of the directional wave spectrum and its spectral tail region. We used an 'exact' version of the weakly nonlinear four-wave interaction source term in the radiative transfer evolution equation for the wave spectrum. We carefully validated cases for which data exists, ensuring that the modeled wave properties, wind input and upper ocean dissipation rates are all consistent with observed levels. This was a key focus of our effort since matching the source term levels over a wide range of wind speeds is essential for reliable forecasts of breaking waves, sea spray and the enhanced air-sea fluxes they generate.

The model output results were evaluated critically in systematic tests from light to severe wind speeds. After extensive iteration and refinement, the model framework is ready for implementation and further testing in operational models. Given that our framework used the 'exact' form of the nonlinear wave-wave interaction**,** we anticipate that the least amount of adaptation and best results will be obtained if the new TSA (Two Scale Approximation) source term for the nonlinear interactions (Resio and Perrie, 2008) is implemented operationally, replacing the standard DIA source term.

An additional goal within this project was to be able to use the forecast breaking wave properties to compute the associated sea spray flux from the modeled breaking wave properties and the wind speed rather than from the wind speed alone. To accomplish this goal, a parallel laboratory study (SPANDEX II) was undertaken to parameterize sea spray flux dependences on breaking wave properties.

Overall, when this project commenced in FY10, existing knowledge on wave breaking was limited, and it was necessary to advance knowledge of the fundamental physics of wave breaking in order to be able to incorporate this process reliably into forecast models. Very significant progress on the scientific fundamentals was achieved during this project in parallel with our modeling effort. The model framework that has been developed for forecasting the breaking wave properties is ready for operational implementation. While detailed knowledge of the physics of very short breaking waves remains incomplete, modeling of these scales is feasible. The capability of including wave breaking properties, especially those of the dominant waves, as part of operational sea state forecasts is now available. This will increase both the accuracy and utility of the next generation of operational coupled sea state and ocean weather forecasting models, particularly in severe to extreme sea states.

TABLE OF CONTENTS

1. BACKGROUND / PROBLEM STATEMENT **5**

1.1 Wave breaking in coupled air-sea interaction modeling

1.2 Wind-wave modeling

1.3 Breaking wave physics and observations

1.4 Wind stress and upper ocean dissipation rate

2. TECHNICAL APPROACH **7**

2.1 Breaking wave observational inputs

2.1.1 Breaking onset dependence on spectral saturation

2.1.2 Spectral dissipation rate source term

2.1.3 Spectral density of breaking crest length and breaking strength parameter

2.1.4 Effective breaking strength b_{eff}

2.2 Modeling objectives and approach

2.2.1 Approach

2.2.2 Modeling benchmarks

2.2.3 Spectral bandwidth of the calculations

3. TECHNICAL ACTIVITIES PERFORMED **11**

3.1 Summary of observational data analysis effort

3.2 Model development and computations

3.2.1 Details of source term development

3.3 Wind and wave model computations

3.3.1 Computations of duration-limited wind wave evolution

3.4 Extraction of breaking wave properties

3.4.1 Breaker crest length per unit area spectral density $\Lambda(c)$ and breaking strength b(c)

3.4.2 Spectral peak wave breaking probability

4. RESULTS AND DISCUSSION **17**

4.1 Benchmark A - Evolution of total wave energy and peak frequency from 3-60 m/s

4.2 Benchmark B - Spectral tail properties

4.3 Benchmark C - Associated wind stress/drag coefficient properties

4.4 Benchmark D - Breaking wave forecasts

4.5 Benchmark E - Overall consistency between wind input and dissipation rates

4.6 Wave model performance - Case study of very young wind sea evolution

4.7 Summary of wave model results

4.8 Sea spray forecasts

4.9 Full coupling of the wave model to the wind field

4.10 Transition to operations

4.11 Highlights of SPANDEX II study

4.12 Benefit analysis summary

4.12.1 Technical output

4.12.2 Strategic implications

Acknowledgements

References

1. BACKGROUND / PROBLEM STATEMENT

In 2010, the National Oceanographic Partnership Program (NOPP) initiated a five-year research project entitled 'Improving Wind Wave Predictions: Global to Regional Scales'. This project was focused on improving operational wind wave modeling, by transitioning new science into such models, and by developing new physics parameterizations for such models. A detailed strategic overview appears in the paper by Tolman et al. (2013) which describes the general goals of the project, the science and operations gaps it attempts to bridge and the data sets and validation techniques for verifying the updated operational models. This report overviews our contribution to this NOPP research initiative.

1.1 Wave breaking in coupled air-sea interaction modeling

Under strong forcing conditions, breaking waves are a conspicuous feature of the wind-driven sea surface, appearing as whitecaps. The impact forcing of large breaking waves provides the greatest safety challenge to shipping and coastal structures. Through their overturning of the air-sea interface, breaking waves profoundly influences the dynamics and thermodynamics of the boundary layers of the upper ocean and the marine atmosphere. Consequences of breaking in the upper ocean surface layer include greatly enhanced observed turbulence dissipation rates in the near-surface region (e.g. Terray et al., 1996; Gemmrich and Farmer, 2004; Sutherland and Melville, 2015). In the atmospheric marine boundary layer, increased wave form drag results from the separated air flow over breaking waves. This is accompanied by augmented sea spray, bubble production and acoustic underwater noise, as well as enhanced microwave backscatter and emissivity. These numerous and diverse aspects of wave breaking are described in greater detail in review articles (e.g. Banner and Peregrine, 1993; Melville, 1996; Sullivan and McWilliams, 2010; Perlin et al., 2013).

Given the important role played in air-sea fluxes by wave breaking, we set out to include this widespread process more explicitly in the next generation of fully-coupled forecast models for the atmosphere-ocean system. The aim of this project was to conduct the research needed to address this challenge, as no such modeling capability was available. Forecasts of breaking wave properties provide valuable practical wave climate information for sea keeping. The approach pursued was to develop more realistic parameterizations for wave breaking occurrence and strength, and to validate them against observations in test-bed models. The end goal was to be able to refine these improvements ready for use in an operational sea state forecasting system, such as WaveWatch III. There are also enhanced scalar air-sea fluxes associated with wave breaking, including sea spray, bubbles and greenhouse gases. Such information is needed to underpin future operational versions of coupled atmosphere-wave-ocean models.

1.2 Wind-wave modeling

In present wind-wave forecast models, breaking waves only appear implicitly as part of the spectral dissipation source term. Otherwise, they receive no direct quantification. These models compute the evolution of the directional wave height spectrum F(k,θ; x,y,t) under the resultant of the spectral source terms, according to the radiative transfer equation (here assuming deep water and no currents):

$$\frac{\partial F}{\partial t} + \vec{c}_g \cdot \nabla F = S_{\mathrm{tot}} \tag{1}$$

where $F = F(k,\theta)$ is the directional wave spectrum, $\vec{c}_g$ is the group velocity. The total source term $S_{tot} = S_{in} + S_{nl} + S_{ds}$, where S_{in} is the atmospheric input spectral source term, S_{nl} is the nonlinear spectral transfer source term representing nonlinear wave-wave interactions and S_{ds} is the spectral dissipation rate, primarily due to wave breaking.

In present-generation forecast models, the wind input term was synthesized from ocean, laboratory measurements and idealized mathematical models. The nonlinear transfer term was derived from weakly nonlinear spectral interactions for an ensemble of irrotational gravity wave Fourier modes (Hasselmann, 1962). The dissipation term was formulated to close the problem and was based on a decay rate formulation controlled by an integral spectral wave steepness parameter.

It should be noted that the source terms in these models are heavily tuned to produce wave height spectral estimates that agree well with corresponding observations. This does not validate the relative strengths of the three source terms, which are more difficult to assess. One option is to compare computed and measured integrated wind input and dissipation rates, for which the integrated nonlinear transfer term vanishes. Unfortunately, neither the integrated wind input or dissipation rate is computed reliably in the models, nor are they easily measured. Hence this approach has not been actively pursued by investigators. However, the recent availability of systematic breaking wave data provides a more robust basis for discriminating between alternative wind input and dissipation rate source terms, and was exploited in this project. Our model validation also depends on detailed comparison of forecast wave spectra with measured high resolution directional ocean wave spectra, which have become available in recent years (e.g. Romero and Melville, 2010).

1.3 Breaking wave physics and observations

This investigation both motivated and generated several significant advances in breaking wave observations and analysis. Prior to this project, available wave breaking field data showed a very large scatter when plotted against standard sea state variables such as wind speed or wave age (e.g. see Figs. 7, 8 in Gemmrich and Farmer, 1999).

This scatter has seen significant reduction over the past two decades. The observational study by Banner et al. (2000) reported a strong correlation of breaking probability of dominant wind waves with their significant steepness above a threshold level. However, an extension of this class of result to the shorter waves in the spectrum was needed. Using the 1999 Pacific Ocean storm waves data [Gemmrich and Farmer (IOS, Canada)], Banner et al., 2002) found a common breaking threshold applicable across different wave scales. This threshold, based on the wave saturation spectrum, contributed a key element of our spectral dissipation rate source term.

A suitable framework was needed to forecast breaking wave properties, which was provided by the spectral density of breaking crest length/unit sea surface area ($\Lambda(c)$) introduced by Phillips (1985). Measurements of $\Lambda(c)$ are now available for a representative range of wind speeds and wave ages through remotely sensed imagery (Kleiss and Melville, 2010; Gemmrich et al., 2013; Schwendeman et al., 2014; Sutherland and Melville, 2015). These results have been of primary importance in calibrating the source terms in this study. A detailed description of $\Lambda(c)$, including available ocean measurements, is given in section 2.1.3. While $\Lambda(c)$ is a key validation variable, it is kinematic in nature. A breaking strength parameter is still needed in conjunction with $\Lambda(c)$, which is also described in detail in section 2.1.3.

1.4. Wind stress and upper ocean dissipation rate

For accurate coupled modeling, the wind stress and upper ocean dissipation rate generated by the wave model need to be consistent with observed levels and their trends with wind speed and wave age. The recent papers by Edson et al. (2013) and Yang et al. (2014) for ocean wind stress and Sutherland and Melville (2015) for the upper ocean dissipation rate, provide excellent observational data for validating the compatibility of wave forecast model capabilities.

2. TECHNICAL APPROACH

We developed a modeling framework and performed numerical model calculations for wind-wave spectral evolution. The output was validated against a set of benchmarks based on field measurements. The source terms were refined iteratively to improve the model performance. Due to the complex nature of the 'exact' nonlinear wave interaction source term, the calculations typically needed 24-48 hours of CPU time to process the evolution to full development. Also, this project required a strong synergy between our modeling effort and basic knowledge of the physics of breaking, including the analysis of field observations. This was an essential element that underpinned our progress throughout this project.

2.1 Breaking wave observational inputs

Fundamental observational contributions on breaking waves generated within this effort were introduced briefly in section 1.3, and are highlighted in section 3.1. Detailed results are described in sections 4.4 and 4.8.

These results materially advanced the development of our goal of including breaking wave physics in our model framework. Key elements were: (i) the formulation and refinement of the spectral dissipation rate source term S_{ds}; (ii) the extraction of spectral breaking wave crest length and strength; (iii) incorporating the strong enhancement of the local wind momentum flux to the waves over breaking waves into the wind input parameterization term (Banner, 1990a; Kukulka and Hara, 2008a,b).

2.1.1 Breaking onset dependence on spectral saturation

A collaborative study (Banner et al., 2002) undertaken with Gemmrich and Farmer at IOS Canada involved a novel scale analysis of breaking waves. This was motivated by the results of the model study of wave breaking onset by Song and Banner (2002), who identified the wave energy convergence rate and geometrical steepening within nonlinear wave groups as key aspects in wave breaking onset. The directionally-normalized spectral saturation $\tilde{\sigma}(f)$ was chosen as a surrogate for local wave nonlinearity. It is given by

$$\tilde{\sigma}(f) = (2\pi)^4 f^5 G(f)/2g^2/\Theta(f) \qquad (2)$$

where f is the wave frequency, G(f) is the wave energy spectrum and $\Theta(f)$ is the directional spreading width spectrum.

Banner et al. (2002) showed that a common breaking threshold based on a spectral wave steepness parameter collapsed the breaking probability data over an appreciable range of wave scales. This parameter underpins our formulation of the dissipation source term and our procedure for extracting breaking wave properties. More specifically, the component of our S_{ds} formulation associated with active breaking associated with a given wave scale bandwidth was

built around the observed normalized saturation threshold. Suitable spectral smoothing was applied to the measurements of normalized spectral saturation $\tilde{\sigma}$.

2.1.2 Spectral dissipation rate source term

We used a refined version of the saturation threshold form of the dissipation rate source term S_{ds} proposed by Alves and Banner (2003), incorporating the observed breaking saturation threshold reported by Banner et al. (2002). Also, various refinements were introduced to shape its spectral distribution, in order to provide a much better match to the wind input source function S_{in} at higher wavenumbers, and to recently published observations of the spectral density of breaking wave crest length/unit area (Kleiss and Melville, 2010; Gemmrich et al., 2013; Sutherland and Melville, 2013).

S_{ds} was composed of a local breaking term S_{ds}^{loc} plus a parametric background dissipation rate S_{ds}^{nonloc} quantifying the effects of longer breaking waves attenuating shorter waves (e.g. Banner et al., 1989) and ambient surface layer turbulence.

The form of S_{ds} used in this study is shown in (3) below. It uses a power law function of the normalized spectral saturation ratio to reflect the observed breaking threshold behaviour, and refines the form proposed by Alves & Banner (2003). The form used here is

$$S_{ds}(k,\theta) = S_{ds}^{loc}(k,\theta) + S_{ds}^{nonloc}(k,\theta) = C[(\tilde{\sigma} - \tilde{\sigma}_T)/\tilde{\sigma}_T)^a + \varepsilon_{res}](\sigma/\sigma_m)^b\, \omega\, F(k,\theta) \qquad (3)$$

where σ and $\tilde{\sigma}$ are respectively the saturation and saturation normalized by the mean directional spreading width, $\tilde{\sigma}_T$ is threshold normalized saturation and σ_m is the saturation at k_m, the mean wavenumber at the transition from the peak enhancement region to the spectral tail.

In (3), the term involving the normalized saturation threshold ratio (left of the + sign) controls the local dissipation rate. The breaking threshold switching exponent *a* was taken as 2 and *b* was taken as 2, based on matching to the high wavenumber forms of the wind input source term $S_{in}(k)$, as discussed below in section 3.2.1.

The coefficient C was chosen to provide the optimal match to observed duration evolution data of the spectral peak energy and peak frequency (e.g. Young, 1999). It is evident that C needs to increase with the wind speed, since the integrated dissipation rate must balance the integrated wind input for developed seas. To achieve this, we used a function of the mean square slope [mss] of the wave field that is wind speed dependent and has a suitably broad dynamic range.

The term ε_{res} in (3) is a nonlocal background dissipation coefficient and its form is not known. We assumed that it scales with the mean steepness parameter Ek_p^2, where E is the total wave energy and k_p is the spectral peak wavenumber. An associated proportionality constant of 0.125 was determined through model runs over the wind speed range 5-60 m/s, for which its performance was found to be effective. This parameterization provides attenuation rates consistent with observed decay rates of swell leaving storm areas (Ardhuin et al., 2009). The measured water-side energy dissipation rate ε in the wave boundary layer is the sum of the two contributions $S_{ds}^{loc}(c) + S_{ds}^{nonloc}(c)$, integrated over all scales and over the depth of the wave boundary layer.

2.1.3 Spectral density of breaking crest length and breaking strength parameter

Spectral density of breaking crest length/unit area Λ(c)

As introduced in section 1.3, the spectral measure of breaking wave crest length, Λ(**c**), has the property that Λ(**c**) d**c** gives the crest length/unit surface area of breaking crests traveling with velocities in (**c**, **c**+d**c**). In this study, Λ(**c**) was one of the primary breaking forecast parameters produced from our modeling effort and was central to validating our source terms and forecast breaking wave properties. A number of allied air-sea fluxes are based on the sea state and wind field rather than on the wind field alone, including breaking wave enhancements to the wind stress and input to the waves, as well as sea spray. These contributions can be quantified through modeled breaking-related properties.

Spectral breaking strength b(c)

A breaking strength measure is needed to quantify the wave energy loss rate through breaking associated with a given Λ distribution. The connection between these two distributions was assumed to be given by the scalar form of equation (6.3) in Phillips (1985), which we generalized to allow the breaking strength coefficient to have a spectral dependence [*b=b(c)*]:

$$S_{ds}^{loc}(c)\,dc = b(c)\,g^{-2}c^{5}\Lambda(c)\,dc \qquad (4)$$

where $S_{ds}^{loc}(c)$ is the spectral energy loss rate from wave breaking, as defined in equation (3).

Underpinning (4) is the assumption that the mean wave energy dissipation rate at scale (c, c+dc) is due primarily to wave breaking in a bandwidth about that scale. This is most likely valid around the spectral peak, however Λ levels for shorter breakers may need to be modified due to the attenuation of short wave energy by longer breaking waves (Banner et al., 1989).

It is noted that the dependence of the spectral breaking strength coefficient b(c) is not well understood. Initial efforts to quantify the breaking strength were based on the Phillips (1985) assumption that *b* is constant for all breaking wave scales. Measurements were made of dissipation rates of narrow-band 2D laboratory breaking waves in focusing packets. These measurements showed a strong dependence of *b* on mean packet wave steepness or energy convergence rate at the packet envelope maximum (Banner and Peirson, 2007; Drazen et al., 2008; Tian et al., 2010). While measurements of *b(c)* in a broad wave spectrum are not presently feasible, recent parametric forms for *b(c)* have been proposed that are based on a spectral analogy of the narrow-banded measurement findings (Romero et al., 2012; Morison and Banner, 2016). These are formulated as a function of the normalized characteristic spectral saturation. The proposed formulation assumes *b(c)* ~ $(\tilde{\sigma} - \tilde{\sigma}_T)^n$, where $\tilde{\sigma}$ and $\tilde{\sigma}_T$ are the normalized spectral saturation and breaking threshold normalized spectral saturation, and n is an exponent to be determined. Further details and results based on this approach are discussed below in section 3.4.

2.1.4 Effective breaking strength b_{eff}

Before proceeding to review our model results against of our proposed suite of performance criteria, we note that the spectral breaking strength *b(c)* has certain complexities, as mentioned above, which can complicate its application. Primarily, *b(c)* cannot yet be measured directly. The only relevant measurements presently available are the total water-side total dissipation rate as a function of depth, hence the best available validation method is indirect. This is discussed in detail in section 4.4 below.

An alternative approach is to use a mean breaking strength coefficient, b_{eff}, defined as

$$b_{eff} = \int S_{ds}^{loc}(c)\, dc \,/ g^2 \int c^5 * \Lambda(c)\, dc \qquad (5)$$

where the integrated $S_{ds}^{loc}(c)$ distribution and $\Lambda(c)$ are either obtained from wave model forecasts or from measurements. The variation of b_{eff} with wave age was investigated recently by us in Zappa et al. (2016), based on measurements and spectral wave model results. This is reported in section 4.4 below.

2.2 Modeling approach and objectives

The overall objective was to refine our model framework to be able reproduce the field-observed benchmarks A-E stated below in section 2.2.2 over a wide range of wind speeds. Further, this refined modeling framework should be suitable for transitioning to operational forecasting in the next generation of coupled atmosphere/sea state/upper ocean circulation models.

2.2.1 Approach

Wave model

We developed a model framework with a spectral dissipation source term S_{ds} based on the threshold nature of breaking. This term was assumed to depend on wave parameters and is underpinned by the saturation threshold behaviour reported by Banner et al. (2002). The approach was based on treating waves in different directional spectral bands as nonlinear wave groups. It belongs to the class of nonlinear forms of S_{ds} discussed by Donelan and Yuan in §II.4 of Komen et al. (1994). This form of S_{ds} provides a method for calculating Λ, the spectral density of breaking crest length/unit area (defined above in section 2.1.3). Details of this form of S_{ds} are given in section 3 below. In addition to the S_{ds} term, we needed a suitable wind input source term, having committed to use the 'exact' form of nonlinear spectral transfer term S_{nl}, in preference to the very approximate DIA version. Special attention was given to ensuring a close match between the total energy flux to the waves and the total water-side dissipation rate in the wave boundary layer.

Wind forcing model

Our strategy in this project was to utilize an accurate wind input source term to drive the model, with an appropriate level of coupling so that future transition to a fully-coupled atmospheric boundary layer model would be straightforward. This required very considerable effort and proved to be very challenging, given the large dynamic range of growth rates in existing wind input source term formulations. In fact, this project was a test-bed for wind input source terms, as our model validation procedure placed stringent demands on this source term for compatibility with the other source terms and matching to observations, as outlined in section 2.2.2. Details of our evaluation procedure and the final form of our wind input source term implementation are summarized in 3.2.1 below.

2.2.2 Modeling benchmarks

A. evolution of non-dimensional mean wave energy E and spectral peak frequency f_p.

B. spectral tail properties: directional lobing; mean directional spreading with k/k_p; spectral saturation; level and exponent of 1D transect k-spectrum (k is the wavenumber, k_p is the spectral peak wavenumber); frequency spectral transition from f^{-4} to f^{-5}.

C. validating the relative size of the computed wave-induced stress levels (non-breaking and breaking) relative to overall wind stress driving the model.

D. prediction of breaking crest length/unit area spectral density Λ and spectral breaking strength b(c) of the wind wave spectrum for different wave ages.

E. ensuring that the modeled integrated water-side dissipation rates match observed levels, and are consistent with the integrated energy flux from the wind to the waves.

2.2.3 Spectral bandwidth of the calculations

We ran broad spectral bandwidth computations of the evolution of the directional wave spectrum and its tail region using an 'exact' version of the nonlinear wave-wave interaction source term S_{ds} in the radiative transfer equation for the wave field. Our S_{ds} needed to be uncompromised by approximations in S_{nl}. We used the 'exact' form of S_{nl} to avoid the known errors associated with 'discrete interaction approximation' implementations in use operationally.

The consequence of using an 'exact' form of S_{nl} was very long computational times throughout the project, due to the millions of interactions that need to be calculated at each space or time step in the evolution. This effect became more pronounced at higher wind speeds, where the time or space step needed to be shortened for stability. At hurricane wind speeds, model runs to well-developed seas required several days to finish. Before proceeding with the calculations, we invested very considerable effort in evaluating various versions of the 'exact' S_{nl} code and propagation/stepping schemes available to us. This was to ensure accuracy and minimize computational instabilities that can develop at higher wavenumbers.

For our standard computations, we concentrated on duration-limited growth cases, which were the least prone to spurious numerical instability. There are established non-dimensional duration-limited growth correlations for wave energy and peak frequency based on field observations (Young, 1999). These can also be inferred from fetch-limited observations by the methodology discussed in Hwang and Wang (2004). In our calculations, a variable logarithmic grid was developed and implemented to accommodate the evolution from very young to very old wind seas over the wide range of wind speeds investigated.

3. TECHNICAL ACTIVITIES PERFORMED

3.1 Summary of observational data analysis effort

(i) we prepared a compilation of all published breaking probabilities of dominant (spectral peak) waves against normalized spectral saturation. This is used to quantify the additional breaking wave stress component in our wind input source function and to provide a validation check of our forecast breaking wave spectral crest density distributions.

(ii) Zappa, Banner, Morison and Brumer (2016) synthesized from the available open ocean data sets a compact form of the dependence of the observed mean breaking strength coefficient b_{eff} against the wave age based on data. This was also used to validate our wave model forecasts of breaking wave properties (section 4.4)

(iii) Fairall, Zappa, Banner, Morison and Peirson (2012) conducted a follow-on laboratory study (SPANDEX II) which significantly refined the breaking wave measurements gathered in SPANDEX I (Fairall et al., 2009), which was the first study seeking to relate sea spray flux directly to breaking wave surface disturbance properties, rather than wind speed. These results

confirmed a strong threshold behavior, with a quasilinear increase in spray flux with breaking energy intensity and near-surface wind speed. This was used in our unified sea spray flux forecast model formulation described in 4.8, with further details of SPANDEX in section 4.11.

(iv) modeling the evolution of the ocean wind wave spectrum depends on the source terms and spectral bandwidth used to compute the governing transport equation. Through detailed measurement, Sutherland and Melville (2015) investigated the relative contributions of breaking wave scales, from large-scale whitecaps to micro-breakers, to the total dissipation rate in the wave boundary layer. They concluded micro-breakers and very small whitecaps contributed a "large fraction of dissipation" and "that a large fraction of wave energy was dissipated by these small breaking waves." In Banner and Morison (2016), we reanalyzed their data and concluded that for young seas, micro-breakers and small whitecaps contribute only a small fraction of the total breaking wave dissipation rate. For older seas, micro-breakers and small whitecaps contribute a large fraction of the breaking wave dissipation rate, but this is only a small fraction of the total dissipation rate, which is now dominated by the non-breaking component. Hence, for all the wave ages observed, micro-breakers and small whitecaps do not appear to make a significant contribution to the total dissipation rate in the wave boundary layer.

3.2 Model development and computations

3.2.1 Details of Source Term Development

A. Spectral wind input source term S_{in}

We used a form of the wind input source term S_{in} with a plausible distribution of wind input to both fast and slower moving waves that provides accurate energy input levels from weak to hurricane forcing conditions, consistent with observational data. We also investigated the sensitivity to the directionality of the wind. We discovered that many forms for S_{in} are non-optimal in our modeling framework if reliable forecasts are sought for wave breaking properties.

The magnitude and spectral composition of the wind input source term S_{in} are imprecisely known, despite very considerable observational and theoretical study over the past few decades. In BM10, we investigated a number of proposed S_{in} formulations: Hsiao & Shemdin (1983); Janssen (1991); Donelan et al. (2006). From our detailed testing, we found that the spectral distribution of the growth rate was crucial to the successful modeling of the breaking properties of the spectral peak waves. With too low a level of input to the dominant waves, there was insufficient excess energy flux to these waves to account for the observed breaking levels. This key factor limited out attention to the Janssen (1991) form for S_{in}, which was modified as discussed in detail in Banner and Morison (2010) through a tail-sheltering modification.

Conceptually, the wave stress driving the shorter waves is reduced from the total wind stress by progressively subtracting the wave stress associated with the longer waves. This approach allowed fine tuning the integrated wind input energy flux to closely balance the integrated energy loss rate due to breaking. This is an important validation check for the modeling, and we found that our sheltering algorithm provided wind stress estimates that agreed very closely with the observed levels as the wind sea aged. The modified Janssen (1991) wind input growth rate was used in S_{in} for all our calculations.

We implemented a modified form of the Janssen (1991) wind input growth rate formulation, with a 'sheltering' term designed to reduce the growth rates to the slower moving, shorter wave components. This was done to maintain the overall aerodynamic drag coefficient at levels consistent with observed levels.

Sheltering strategy

The total aerodynamic drag is the sum of the wave drag, the breaking wave drag and the tangential stress, i.e.

$$\tau_{tot} = \tau_w + \tau_{bw} + \tau_{\text{tang}} \tag{6}$$

The wave stress is expressed as:

$$\tau_w = \iint [\gamma F(k,\theta)/c]\, k dk d\theta\,, \tag{7}$$

where the growth rate γ is given below.
The breaking wave stress is expressed as:

$$\tau_{bw} = \int \tau_{bw}(\mathrm{k}) dk = \int \mathrm{Pr}_{br}(\mathrm{k}) * Fr(\mathrm{k}) * \tau_w(\mathrm{k}) dk\,. \tag{8}$$

Here, $\mathrm{Pr}_{\mathrm{br}}(\mathbf{k})$ is the breaking probability at scale **k** and Fr(**k**) is the ratio of actual crests to Fourier modes at scale **k**. For details on how $\mathrm{Pr}_{\mathrm{br}}(\mathbf{k})$ and Fr(**k**) are defined and parameterized based on observations, see Banner and Morison (2010).
The tangential stress parameterization is expressed as:

$$\tau_{\text{tang}} = \mathrm{A}\,\rho_{\text{air}}\,\mathrm{U}_{10}^2 \quad \text{with} \quad A = \max\left[10^{-5}, 1/(\mathrm{t}_1\,\mathrm{U}_{10}^{\mathrm{t}_2})\right], \text{ where } \mathrm{t}_1 = 325,\ \mathrm{t}_2 = 0.9.$$

This was based on the tangential drag coefficient behaviour reported by Banner and Peirson (1998). They observed that the tangential drag coefficient was a decreasing function of the wind speed, largely independent of the wave age. We developed a parameterization that conformed to their data trend at moderate wind speeds, and asymptoted to a residual level of 0.0001 for hurricane winds of 50 m/s**.** This is based on the assumption that no matter how strong and widespread the air flow separation becomes, the wind always maintains some residual re-attachment to the water surface, where the tangential stress will be non-zero.

In the present modeling, the overall friction velocity is given by $u_* = \sqrt{\tau_{tot}/\rho_{air}}$. Also, a reduced friction velocity felt by the nth wavenumber $\mathrm{k_n}$, which reflects the sheltering of the short waves by the longer waves, is given by

$$u_*^{red}(k_n) = \sqrt{\tau_{tot} - \alpha_{sh}\sum_{i=1}^{n}(\tau_w(i) + \tau_{bw}(i))\Big/\rho_{air}} \qquad \text{for } 1 \le \mathrm{n} \le \mathrm{N} \tag{9}$$

where N is the total number of wavenumber grid points. At each timestep, the model recalculates the total and local u_* levels, which are then fed back into the wind input source term. This key aspect of the wind input source term is described in the following section. Here α_{sh} is a constant that reflects the level of sheltering. This parameter allows setting the sheltering level to obtain an optimal match between the wind stress generated in the model and the observed level as a function of wind speed and wave age.

Modified Janssen (1991) wind input growth rate formulation

Following Janssen (1991), we define:

$$\mu = (u_*/\kappa c)^2 (g z_0 / u_*^2) \exp(J_1 \kappa / (u_* \cos\theta / c)^2)\,, \tag{10}$$

where $\kappa = 0.4$ is the Karman constant, $J_1 = 0.99$, c is the phase speed and θ is the direction of the waves relative to the wind.

The Miles parameter (Miles, 1957) is given by:

$$\beta = J_2\,\mu\left(\ln(\mu)\right)^4/\kappa^2,\ \text{for}\ \mu \le 1\ \text{where}\ \ J_2 = 1.6. \tag{11}$$

$$\beta = 0\ \text{for}\ \mu > 1.$$

The spectral growth rate is then given by:

$$\gamma(k,\theta) = \varepsilon\beta\omega\,(\mathrm{u}_*^{red}(k)/c)^2\cos\theta, \tag{12}$$

where ε is the ratio of air to water densities, and the corresponding wind input source term is:

$$\mathrm{S_{in}} = \gamma\,F(k,\theta). \tag{13}$$

Fig.1 below illustrates the typical impact of the sheltering in relation to the Janssen91 growth rate as well as to other proposed growth rate formulations (Snyder et al., 1981; Hsiao and Shemdin, 1983; Plant, 1990), for reference. Note that the form of the Janssen (1991) growth rate parameterization has been largely followed, with the Miles coupling parameter based on the overall u_*/c, but input to the shorter waves modified by using u_*^{red} in the quadratic forcing term.

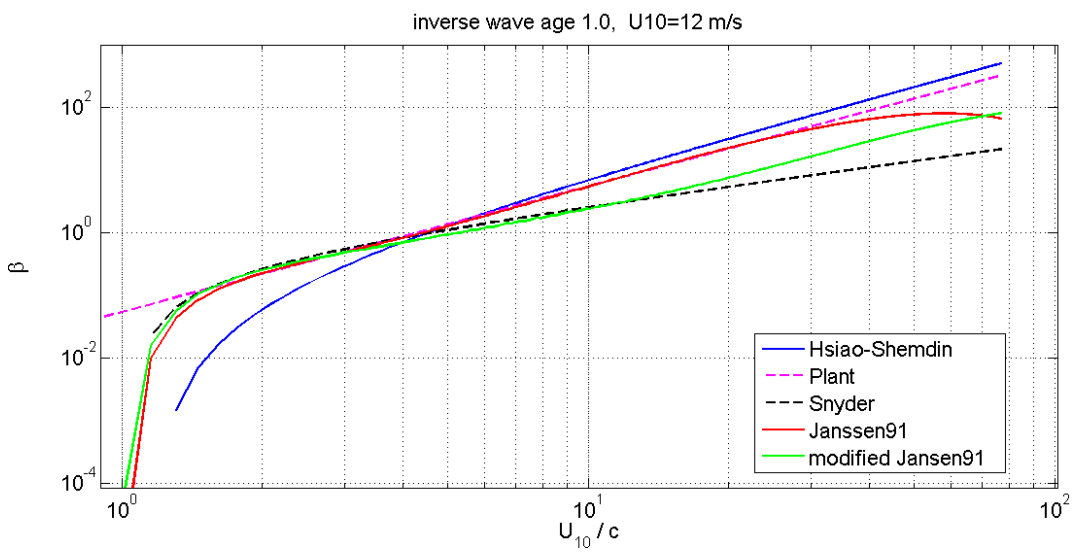

Figure 1. This logarithmic plot highlights the considerable differences between the spectral growth rate β of selected proposed forms of S_{in}. The differences are shown for maturing seas (U_{10}/c_p~1.0). The modified Janssen91 curve shows the extent of sheltering introduced for the slower moving, shorter waves needed to bring the computed wind stress into agreement with observed levels.

B. Spectral nonlinear transfer rate source term S_{nl}

The version of 'exact' S_{nl} used was a recent update (Don Resio, private communication) of Tracy and Resio (1982) with ±180° directional coverage. Our decision to run a wide spectral bandwidth required careful testing for high wavenumber instabilities and was expensive in both development and computational time. The instabilities were minimized by using short timesteps, and initial dampening of rates of change. Also, energy removal at high wavenumber end of the grid achieved by imposing a k^{-4} tail termination on the computed solution, thereby suppressing any accumulation at the end of grid associated with S_{nl}. The model output verified that the nonlinear transfer term had zero net integral at all times.

C. Spectral dissipation rate source term S_{ds}

The form of S_{ds} used in this study was described in detail in section 2.1.2, and was stated as equation (3):

$$S_{ds}(k,\theta) = C[(\tilde{\sigma} - \tilde{\sigma}_T)/\tilde{\sigma}_T)^a + \varepsilon_{res}](\sigma/\sigma_m)^b \, \omega \, F(k,\theta) \tag{14}$$

The power law function of the normalized spectral saturation ratio reflects the observed breaking threshold behavior. Where the normalized spectral saturation falls below the threshold, the local dissipation no longer arises from wave breaking. This proposed form (3) for S_{ds} refines the integral wave steepness threshold used in the quasilinear form of S_{ds} presently used in many operational sea state forecast models.

3.3 Wind and wave model computations

We assumed a neutrally stable logarithmic atmospheric boundary layer structure over the sea.

$$U(z) = \frac{u_*}{\kappa} \log\left(\frac{z}{z_0}\right) \tag{15}$$

The wind-wave model was initiated with a JONSWAP spectrum at a suitably short fetch, depending on the wind speed. Changes in the background wind field due to the waves impacted the wind stress that forced the wave model. This was subject to numerical control during the spin up period.

3.3.1 Computations of duration-limited wind wave evolution

Computations of the directional wave spectrum were made for the spectral bandwidth covering gravity waves from 0.01 Hz up to 5 Hz, using the source terms described above. We focused our development initially on the case of a steady forcing wind speed of U_{10} = 12 m/s. This corresponded to available observations where data on winds, waves and breaking waves were gathered simultaneously and could be used for detailed validation. Once this case had been optimized, model evolution runs were carried out for wind speeds from 3 - 60 m/s, and ran stably up to 100m/s.

Benchmark D (section 2.2.2) proved to be particular strategic significance. This involved a comparison of forecast and observed breaking wave properties during growing seas especially at the spectral peak where the proposed relationship (4) is most likely to be valid. Not only does this provide a tighter constraint on the form of the spectral dissipation rate source term, but it has the benefit of reducing the uncertainty in the form of S_{in}, as discussed below.

We implemented and refined our modeling strategy for extracting the relevant wave breaking parameters, evaluating the wind stress components and coupling the wind and wave models so that a feedback was operative in which the computed wind stress forced the wave model interactively. Concurrently, we investigated breaking wave properties, validating the results using newly available breaking wave data.

3.4 Extraction of breaking wave properties:

3.4.1 Breaker crest length per unit area spectral density Λ(c) and breaking strength b(c)

Banner and Morison (2010) described in detail how b and Λ at the spectral peak can be extracted from the numerical calculations of $S_{ds}^{loc}(\boldsymbol{k})$ and normalized spectral saturation $\tilde{\sigma}$. In this project, we refined this capability to compute b(c) and Λ(c) over the full spectral scale bandwidth resolved in the model.

We followed an approach similar to Romero et al. (2012) which mimics spectrally the observed breaking strength dependence on wave steepness reported in laboratory breaking wave studies of Drazen et al. (2008), but uses our normalised spectral saturation to mimic this in the spectrum. After adjustment to obtain the equivalent spectral form using our open ocean normalized saturation breaking threshold, we defined the breaking strength parameter as:

$$b(c) = H(\tilde{\sigma} - \tilde{\sigma}_T) * A_{br} * \left(\tilde{\sigma}^{0.5} - \tilde{\sigma}_T^{\,0.5}\right)^{1.0} \tag{16}$$

where A_{br} = 0.0025 is a breaking strength coefficient. The corresponding breaking crest length distribution then follows from (5). Hence

$$\Lambda(c) = S_{ds}^{loc}(c) * g^2/(b(c) * c^5) \tag{17}$$

Thus $\Lambda(c)$ is derived from our modeled $S_{ds}^{loc}(c)$ and (16) for b(c), so verifying $\Lambda(c)$ validates $S_{ds}^{loc}(c)$ and b(c). Note that A_{br} is determined empirically through matching modeled and observed B effective levels.

This post-processing spectral breaking formulation allows the breaking strength and crest length distributions of the waves to be forecast from the output of a spectral wave model. However, there are potential sensitivities that need to be taken into account as they can affect the accuracy of the extracted breaking properties. They are associated with the rapid variation of the normalized spectral saturation $\tilde{\sigma}$ and local dissipation rate in the vicinity of the spectral peak, together with the spectral dependence of b(c).

As the project progressed, we were able to significantly refine our capability for calculating the spectral density of mean breaking wave crest length/unit area $\Lambda(c)$ to the point where close agreement was achieved between modeled and observed levels of breaking probability for the dominant waves for both developing and maturing seas (see section 4.4 below). Also, the recent availability of microscale breaking data from infrared measurements (Sutherland and Melville, 2013, 2015), provided better detection and resolution of the very short breaking waves in the spectral wavenumber tail which may not entrain air. Our model results are able to capture their behavior reasonably well, as discussed in section 4.4 under 'Breaking wave forecasts'.

3.4.2 Spectral peak wave breaking probability

We were able to verify the model forecasts of $\Lambda(c)$ independently of b(c) by comparing dominant wave (spectral peak) breaking probabilities calculated from the forecast $\Lambda(c)$ against observed levels, and validate our best fit parameterisation for breaking probability against normalized spectral peak saturation, using:

$$Pr_{br}(c) = \int_{0.7c_p}^{1.3c_p} c\Lambda(c)dc \Big/ \int_{0.7c_p}^{1.3c_p} c\Pi(c)dc \tag{18}$$

where c_p is the spectral peak phase speed. This represents the ratio of breaking crest passage rate to the passage rate of all crests in the spectral peak region. In Appendix A in Banner and Morison (2010), it is shown that the denominator is well-approximated by 0.6 $g/(2\pi c_p^2)$. From the modeled spectral evolution, the spectral peak breaking probability can be computed for any wind and wave age, and the results compared with the ensemble of currently available observations. The breaking probability correlation against normalized saturation for the data we compiled, as well as our model parameterization used in calculating the breaking stress is shown in Fig.2, below. Validation of model results for breaking properties against this data calculated using equation (18) is discussed in section 4.4 below.

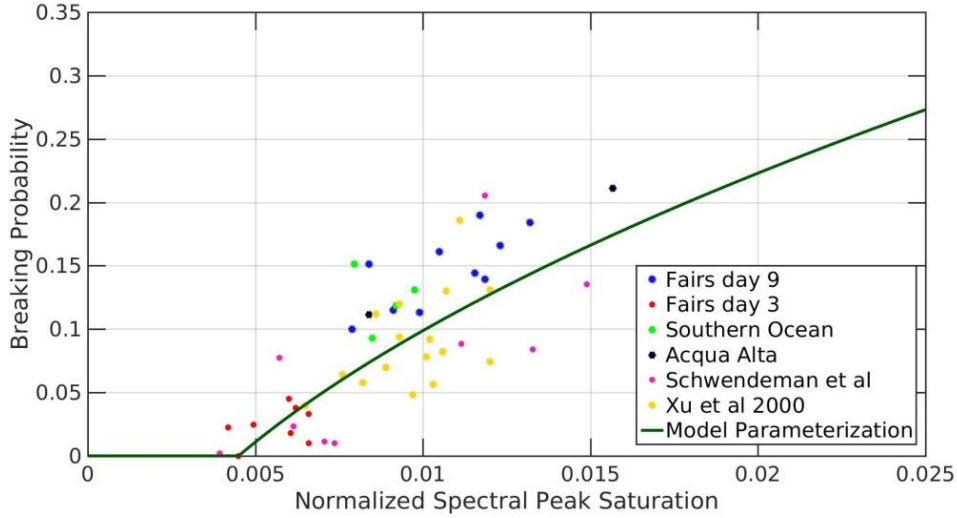

Figure 2. The parametric relationship (solid black curve) used in our model to estimate the additional breaking wave stress in the computed wind stress, was obtained as a fit to the measured data (colored circles).

4. WAVE MODEL EVOLUTION RESULTS AND DISCUSSION

We began by validating our model results for wave energy and spectral peak frequency against the duration-limited data trend curve given by Young (1999, §5.3.4) (benchmark A in section 2.2) at U_{10}=12 m/s. The model diagnostics for U_{10}=12 m/s were very encouraging, so we carried out model runs over a very wide range of wind speeds from 3-60 m/s to investigate the robustness of our model performance. It is important to note that the model settings were not modified for the higher wind speed cases explored, nor were any limiters used to constrain the results. Thus benchmark A was met in terms of closely matching the evolution of the standard growth curves over the entire wind speed range investigated (3 to 60 m/s), as seen in Fig.3.

4.1 Benchmark A - Evolution of total wave energy and peak frequency from 3-60 m/s

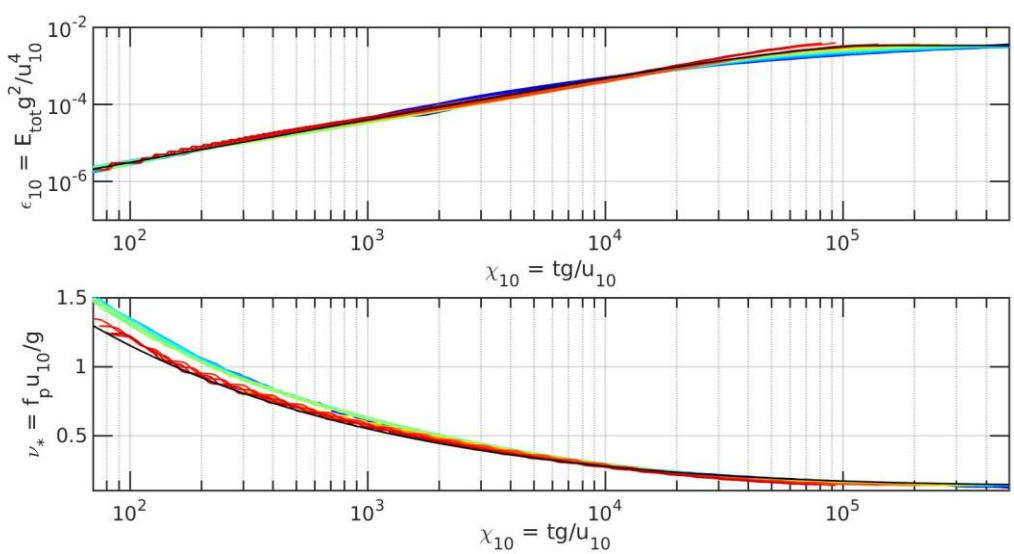

Figure 3. Evolution of non-dimensional mean wave energy (upper panel) and spectral peak frequency (lower panel) against non-dimensional time for duration limited growth under 3-60 m/s wind forcing. The background dashed lines are the trends of the data collated by Young (1999).

4.2 Benchmark B - Spectral tail properties

The results for benchmark B in section 2.2 are shown in Figs. 4 and 5. These spectral measures have been checked carefully against available data and are in close agreement.

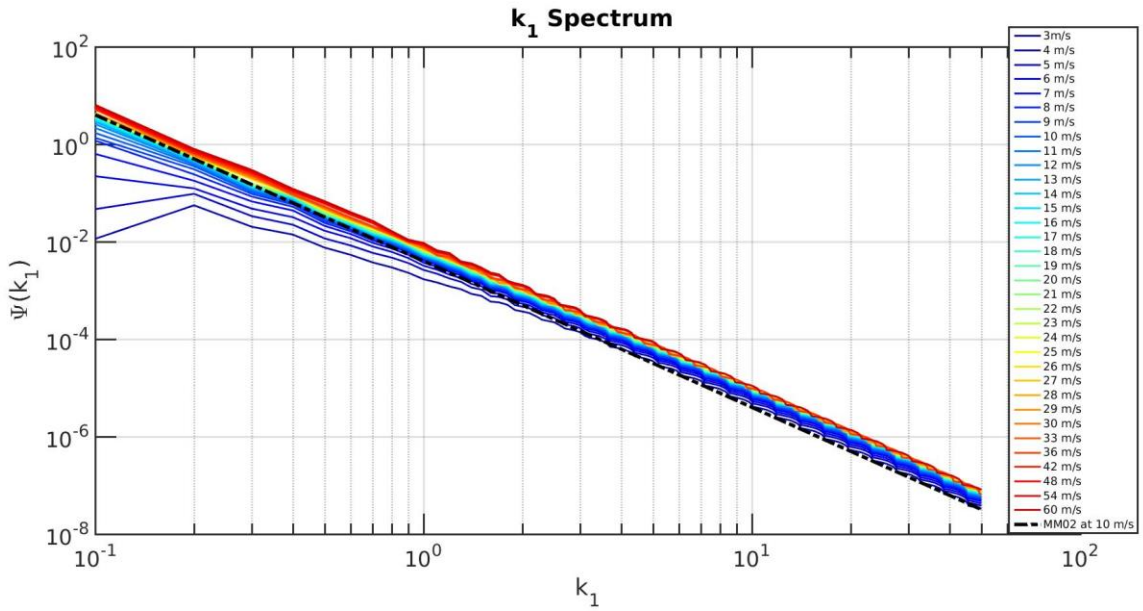

Figure 4. One-dimensional (k_1) wavenumber transect spectra in the upwind-downwind direction, for wind speeds from 3 to 60 m/s for a range of wave age conditions. The dashed black line is k^{-3}.

One-dimensional transect wavenumber spectrum

Computed one-dimensional (k_1) wavenumber transect spectra in the upwind-downwind direction are shown in Fig.4 for U_{10} ranging from 3 to 60 m/s for a range of wave age conditions. These spectra show a close correspondence with the measured k_1^{-3} tail exponent and weak wind speed dependence reported by several studies (e.g. Romero and Melville, 2012).

Directional spreading properties

The directional spreading of the spectrum is an important feature that has been measured reliably in recent years, and is an important feature for source term balance validation. Fig. 5 shows the directional spreading at different k/k_p for a range of wind speeds (12 m/s. 24 m/s, 36 m/s and 48 m/s and two wave ages, corresponding to young seas and to mature seas.

Characteristically single-peaked near the spectral peak, these directional spreading distributions develop a distinctive bi-modal peak towards higher k/k_p with maxima exceeding up to ±50 degrees off the primary wave direction, and lobe ratios up to 1.2. The variability with respect to k/k_p, wind speed and wave age can be assessed from these results and compared with available data. The comparison is generally very favourable, but maximum measured lobe ratios tend to be higher than our modeled levels. The S_{nl} term is at the heart of the lobed spreading distribution, and our results suggest that the form of S_{nl} used may need some refinement in order to match the lobe ratio data more closely. However, this is regarded as of secondary importance.

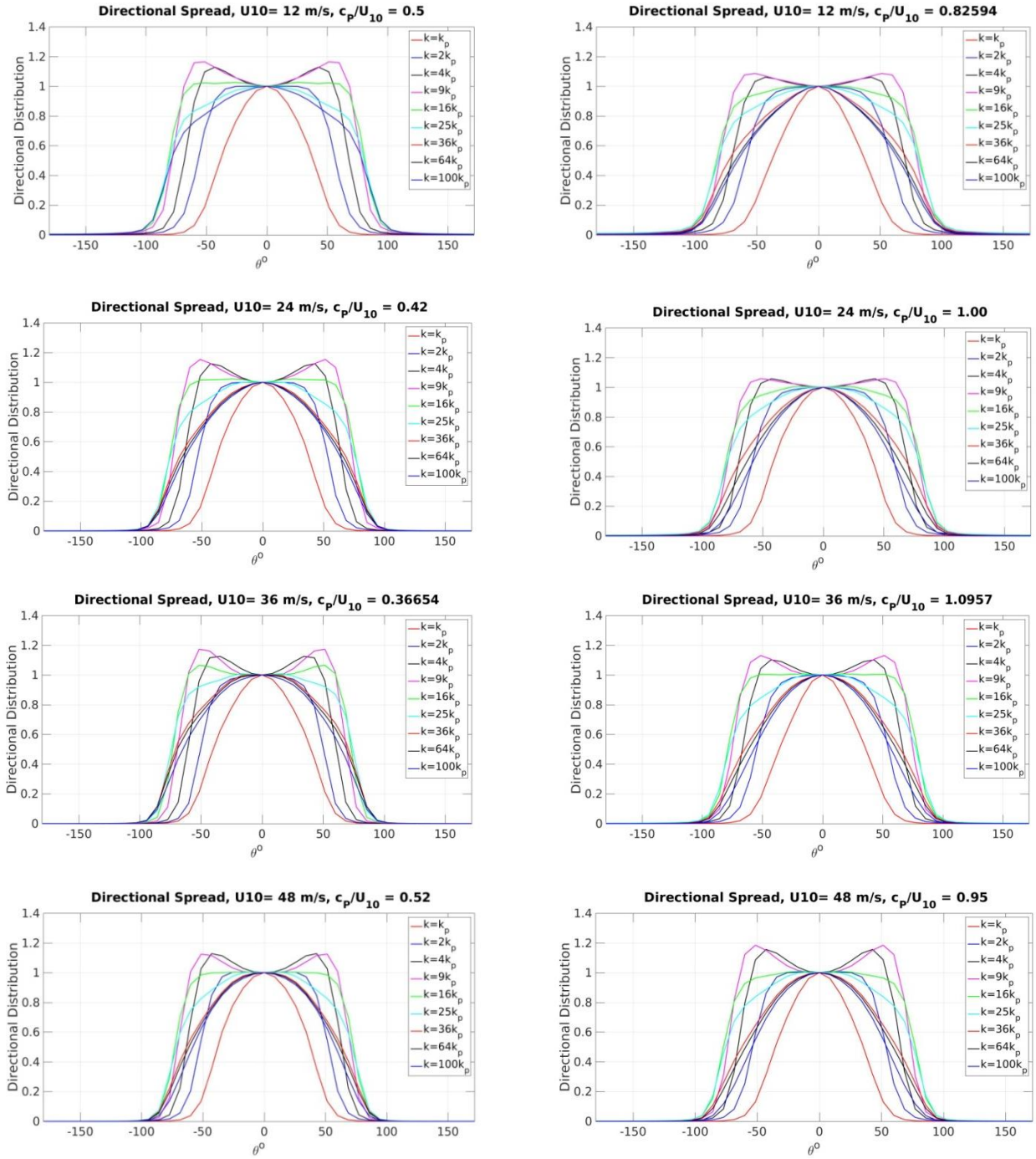

Figure 5. The eight panels show directional distribution of wave energy with distance from the spectral peak for 12, 24, 36 and 48 m/s forecasts. The left panels are for younger seas, and the right panels are for older seas.

Mean directional spreading

The directional spreading angle is defined as:

$$\bar{\theta} = \int \theta F(k,\theta) k dk d\theta \Big/ \int F(k,\theta) k dk d\theta \tag{19}$$

Fig.6 shows the modeled variation of the mean directional spreading angle with distance from the spectral peak for wind speeds 3-60 m/s for young seas, mature seas and for a full range of wave ages. It also shows these results for 4-16 m/s wind speeds and wave ages against data from Romero et al., 2010. The last panel shows the close agreement between forecasts and data.

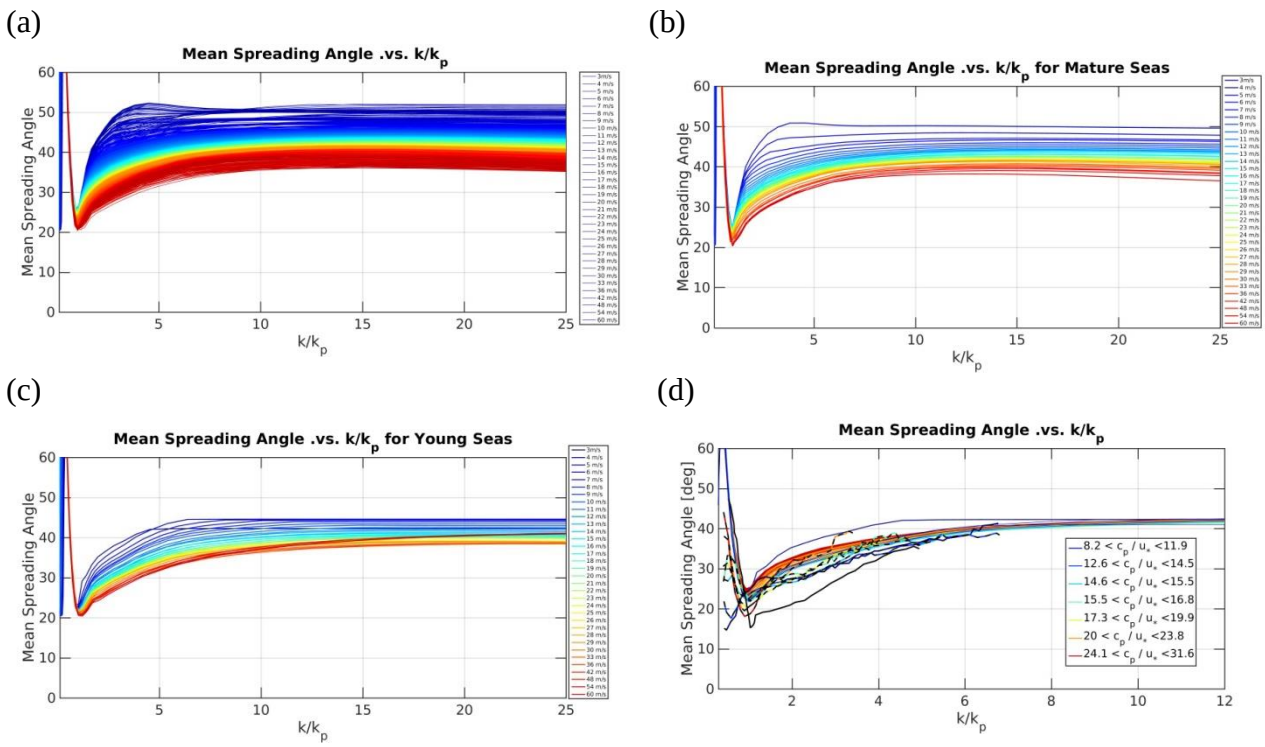

Figure 6. Modeled variation of the mean directional spreading angle with distance from the spectral peak. (a-c) for wind speeds 3-60 m/s for (a) young seas; (b) mature seas and (c) for a full range of wave ages. (d) mean spreading angle for 4-16 m/s matching wind speed and wave ages with data from Romero et al., 2010, with the matching data plotted in heavier black-dashed lines.

Normalized spectral saturation

The normalized spectral saturation $\tilde{\sigma}$ defined in section 2.1.1 is used in the formulations of the local dissipation and breaking strength parameters. Fig.7 below shows its variation with k/k_p for the wind speed ranging from 3-60 m/s for two wave age cases, corresponding to young and mature wind seas. Also shown is the breaking threshold level of $\tilde{\sigma}$ found by Banner et al., 2002 and used in our modeling.

It is noted that this parameter is akin to the classical 'ak' slope steepness parameter that serves as a measure of nonlinearity in wave analysis. While a geometric parameter, it is the closest surrogate that has been proposed to date for parameterizing the nonlinear dynamics/energetics of wave trains in a spectral context.

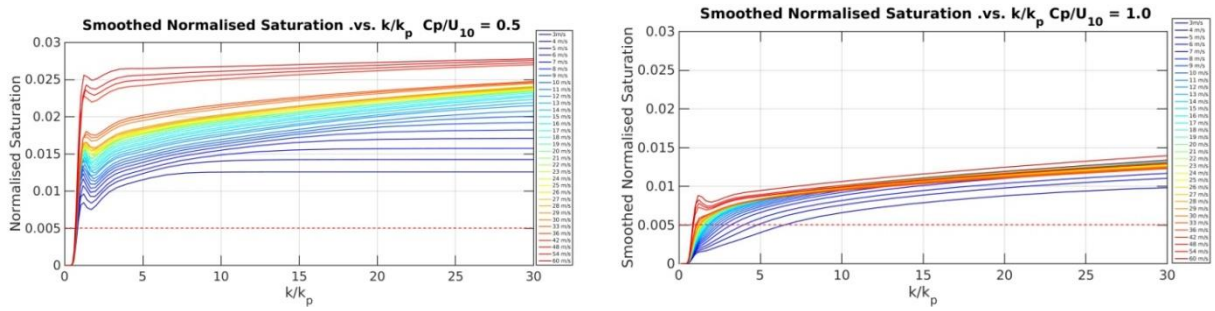

Figure 7. Plots of the behavior of the normalized saturation against k/k_p for wind speeds 3 to 60 m/s. The red dashed lines shows the threshold used in the local dissipation source term. Left panel is for young seas, right panel for older seas.

Frequency spectrum tail transition

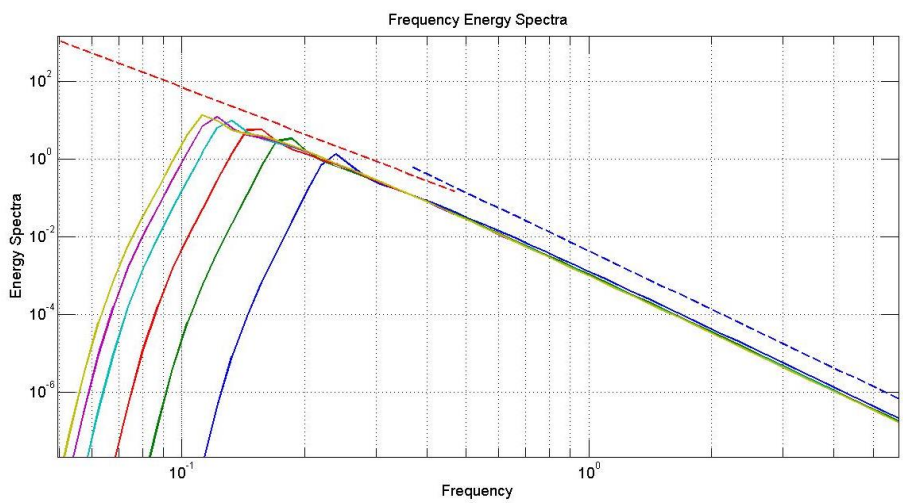

Figure 8. Computed frequency spectra at different stages of development for U_{10}=12 m/s. Red and blue dashed lines have exponents -4 and -5 respectively.

The frequency spectra computed from the modeled directional wavenumber spectra show the tail slope transitioning from f^{-4} to f^{-5} at about 3 times the spectral peak frequency. This behavior is also seen in many wave measurements using single-point instruments such as buoys or wave poles. This phenomenon is due to the increasing directional spreading with distance from the spectral peak, as first explained by Banner (1990b).

4.3 Benchmark C - Associated wind stress/drag coefficient properties

Benchmark C (section 2.2.2) is concerned with the relative size of wave-induced stress level. The sum of the wave stress (non-breaking and additional breaking contributions) and the viscous tangential stress equals the total wind stress. The most recent comprehensive open ocean data for measured sea surface drag coefficients (Edson et al., 2013) covers the wind speed range 5-27 m/s and a subset of wave age conditions of the computations.

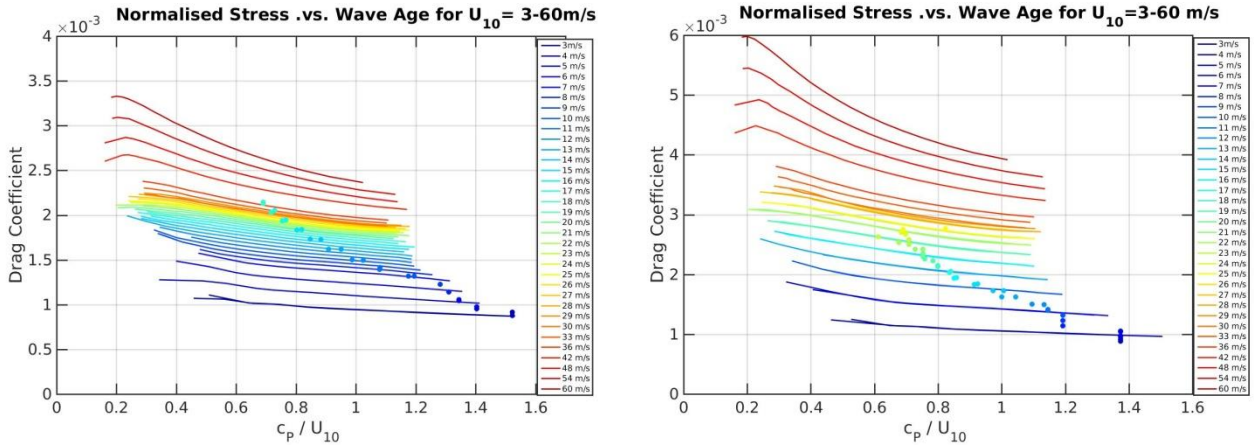

Figure 9. Behavior of the sea surface drag coefficient with wave age for wind speeds from 3-60 m/s during the evolution from young to old wind sea conditions. The superimposed data show measured sea surface drag coefficients from Edson et al. (2013). The color code for wind speed is seen in the legend. The left panel has α_{sh} =0.95 and the right panel has α_{sh} = 0.85.

The model results shown in Fig.9 agree closely with these observed levels and indicate likely levels when extrapolated beyond the measured ranges. These two figures illustrate the sensitivity to the size of the sheltering coefficient α_{sh}. It is seen that reducing α_{sh} from 0.95 to 0.85 improves the agreement between modeled and observed trends, but appreciably increases the drag coefficient for very high wind speeds. As there is no drag coefficient data available yet for these extreme winds for conventional large fetch (non-hurricane) conditions, the optimal choice of α_{sh} remains an open question.

Normal and breaking wave stress contributions to the wind stress

As discussed above in section 3.2.1, the total wind stress is modeled as three additive components: the wind stress associated with wind momentum flux to the waves ('wave stress'), a wave stress enhancement associated with separated wind flow over breaking waves, plus a viscous tangential stress component, usually small. The modeled behavior of the first two contributions is shown in Fig.10 below, which indicates their relative importance at different stages of development for wind speeds ranging from 3-60 m/s.

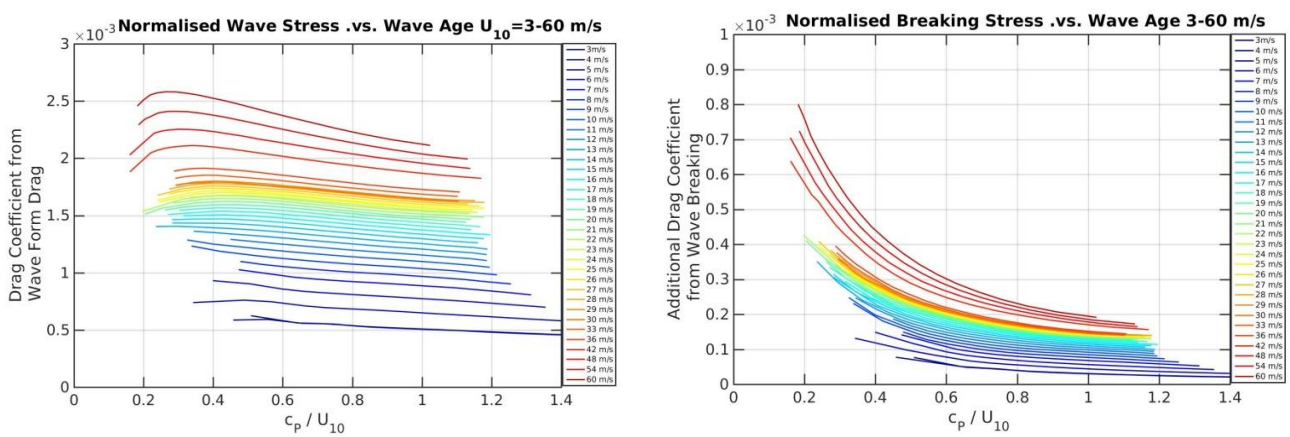

Figure 10. Variation with wave age of the normalized wave stress (left panel) and additional breaking wave stress (right panel) for the wind speed ranging from 3-60 m/s. These combine with the viscous stress to obtain the total momentum flux to the sea surface from the wind.

4.4. Benchmark D - Breaking wave forecasts

Spectral density of breaking crest length/unit area

A major aspect of our model validation sought to reproduce observed breaking wave statistics.

The most recent comprehensive open ocean measurements of Λ(c) were reported by Kleiss and Melville (2010), Romero et al. (2012) and Sutherland and Melville (2015). For the slower-moving shorter breakers, previous visible video imagery data showed an unexplained strong attenuation of Λ below c=3 m/s. However, the recent resolution and sensitivity advances in infra-red video capability for imaging breakers, including non-aerating microscale breakers. This has allowed extending the slow-moving breaker range significantly (Sutherland and Melville, 2013, 2015). So the higher resolution Λ(c) observations more closely match the shape and level produced by the model. Further enhancements in measurement techniques may reduce the difference in Λ(c) for speeds below 1 m/s.

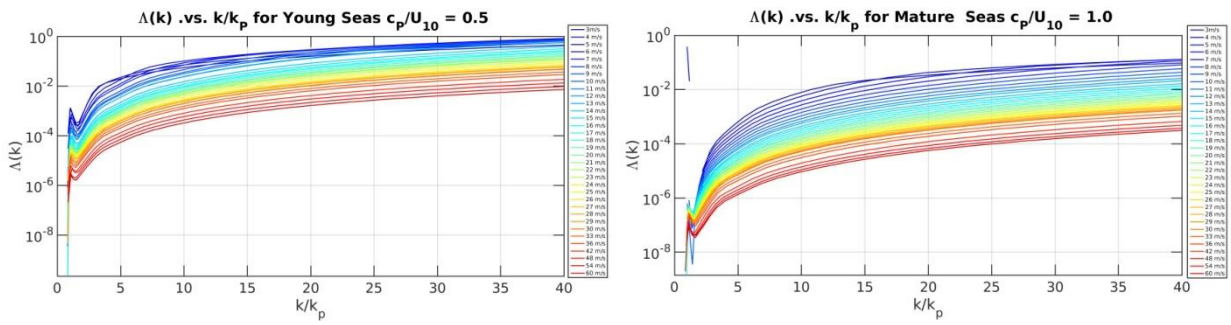

Figure 11. Breaking crest length per unit area of sea surface [Λ(k)] versus k/k_P for young seas (left) for wind speeds 3 to 60 m/s and for mature seas (right).

The Λ(k) measurements show consistently high levels of Λ in the tail, and an enhanced Λ around the spectral peak enhancement region. Also as the seas mature, the spectral levels of Λ in the spectral peak region reduce significantly. However, to date, no reliable observations of Λ(k) are available, and so we will look at Λ(c) and b(c) in the wave speed domain, where reliable Λ(c) measurements have been made.

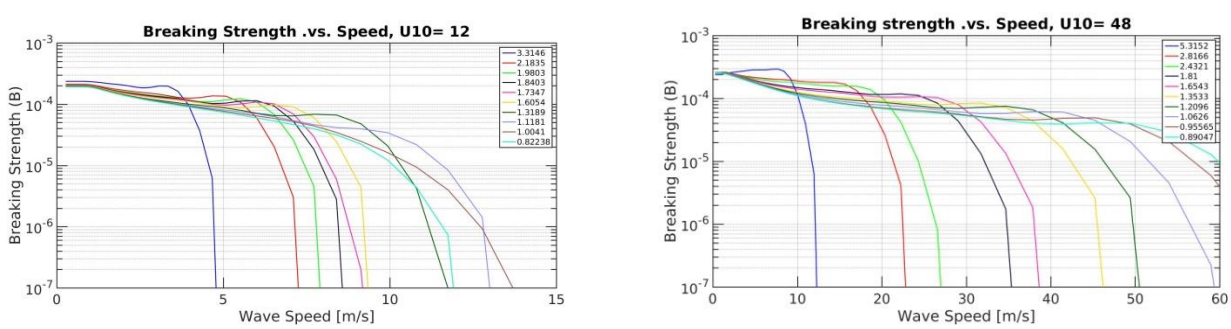

Figure 12. Breaking strength b(c) versus wave speed c, for different wave ages (U_{10}/c_p) for 12 m/s (left) and 48 m/s (right).

The breaking strength is weakly dependent on wind speed, but significantly dependent on wave age and wave speed. There are no observations for b(c), largely because it is difficult to measure the speed (or wavenumber) dependence of the local wave dissipation. We can validate the

effective breaking strength in observations using the integrated dissipation and integrated Λ distributions, and this is shown in Fig.16 below.

A number of observational data sets have been collected for Λ(c), and recently this has been extended into the shorter waves, using infrared video by Sutherland and Melville (2015). Fig.13 below shows the forecasts of Λ(c) from the model, matching wind speed and wave age ranges with the data from Sutherland and Melville (2015).

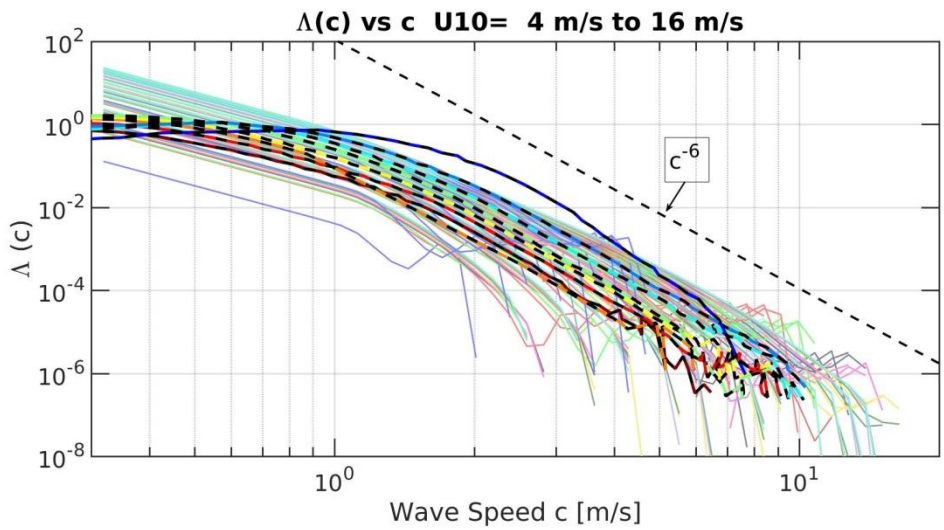

Figure 13. Plots of breaking crest length per unit area (Λ(c)) versus wave speed (c) for model runs 4-16 m/s matching the wind speed and wave age range of Sutherland and Melville (2015). The matching observational data is plotted in thick black-color dotted lines, with the colors of both the observations and the model data matching the wave ranges from Sutherland and Melville (2015).

The results indicate very encouraging agreement between observed and forecast levels during developing sea state conditions. For 'fully-developed' seas, the model produces no breaking at the spectral peak. The observations start to roll away from the c-6 slope below about 2m/s, and the roll over totally below 1 m/s. While the model slope similarly decreases below 2 m/s, the model Λ(c) never rolls over. However, this discrepancy is not energetically significant. This difference may be due to deficiencies in either the very tail of the model, or the tail of the observations, and further enhancements in observation capability or in our understanding of the physics of short breaking waves may remove this minor discrepancy in the future. Clearly, further comparisons with data are now needed to establish the robustness of the modeling approach proposed here.

While further field observational validation is required, the agreement of these initial results is very reassuring. To the extent possible, this phase of our effort met our modeling benchmark D.

Breaking probability data analysis results

Banner et al. (2002) reported an analysis of breaking probability with scale based on using the directionally-normalized spectral saturation $\tilde{\sigma}(f) = (2\pi)^4 f^5 G(f)/2g^2/\Theta(f)$, where f is the wave frequency, G(f) is the wave energy spectrum and Θ(f) is the directional spreading width

spectrum. Their results revealed a remarkable near-uniform collapse for the breaking probability in different spectral bands at and above the spectral peak waves. They highlighted a common threshold for $\tilde{\sigma}(f)$ of approximately 4.5×10^{-3} for breaking onset and established order into the analysis of breaking wave measurements for the first time.

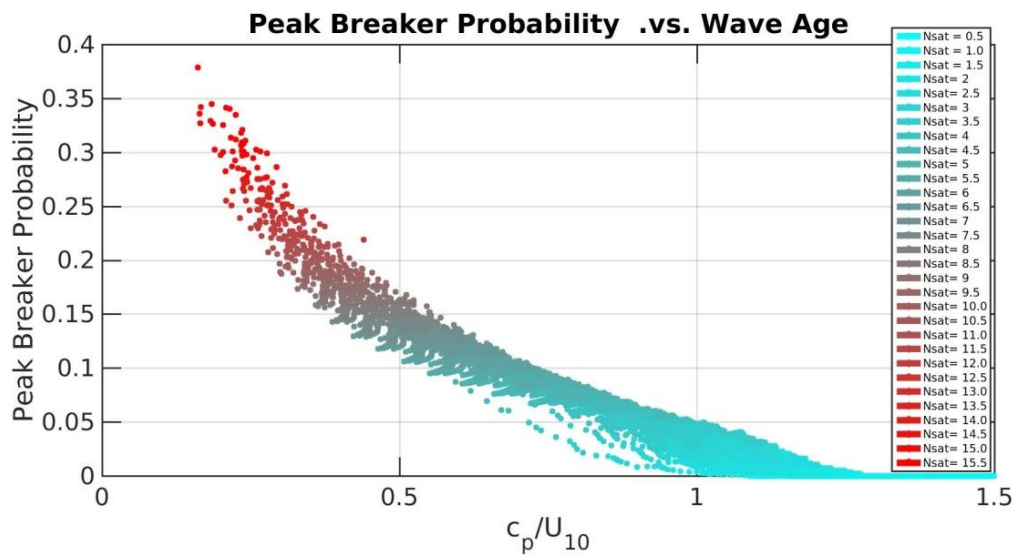

Figure 14. Breaking probability for the dominant wind sea, calculated using equation (18), versus wave wage for U_{10} = 3 to 60 m/s. The color coding refers to the normalised saturation (Nsat=$\tilde{\sigma}$) shown in the legend.

As described in detail above in section 3.2.1, our present study used a formulation for S_{ds} for the dissipation rate associated with wave breaking based on this observed normalized saturation threshold. As part of the wind input source term, there is a component associated with additional wave form drag over breaking waves associated with the separated flow they induce. This additional wind input contribution is parameterized spectrally using the breaking probability with wave scale.

Once $\Lambda(c)$ has been calculated, the peak breaking probability is obtained using equation (18). Fig.14 above shows the variation of spectral peak breaking probability against inverse wave age for a range of wind speeds and normalised saturations. From this, it is seen that the spectral peak breaking probability is a strong function of both wave age and normalized saturation, which is expected based on equation (16) and the relationship between normalized saturation and wave age. Further, there is no indication of significant wind speed dependence, suggesting that breaking probability is much more a function of sea state than wind speed.

The self-consistency of the breaking probability parameterization used as part of the input source term is verified from the computed breaking properties output from the model for the dominant (spectral peak) waves, where such data is available. Fig.15 below shows close agreement for the breaking probability against normalized spectral saturation between our parametric data-fit curve, our model forecasts using equation (18), and observation of breaking probability.

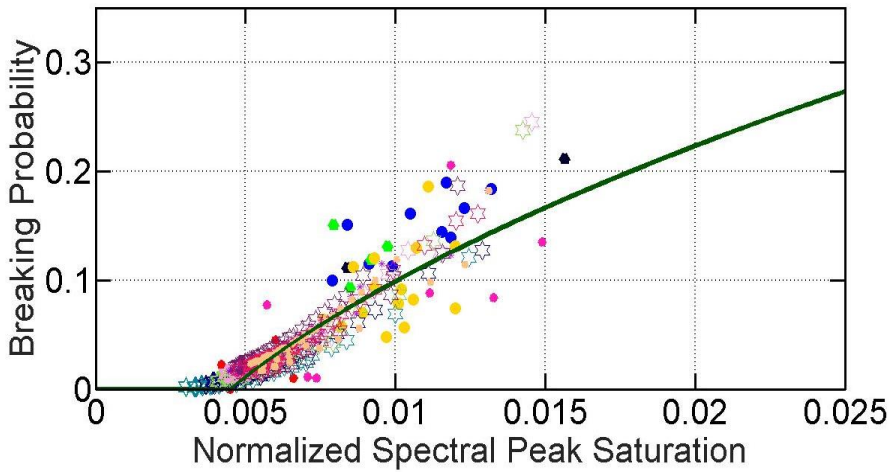

Figure 15. The observed breaking probabilities (colored circles) are plotted against observed normalized saturation, as well as our computed breaking probabilities (open stars) from the model using equation (18). The model forecasts show a close correspondence with the observed data and the data-fit parametric curve (solid line) also shown earlier in Fig. 2. This validates the parametric relationship assumed in our model to quantify the additional contribution of wave breaking to the computed wind stress shown in Fig.10 above.

Effective breaking strength b_{eff}

As discussed earlier in section 2.1.4, we compiled a plot of the variation of b_{eff} with wave age c_p/U_{10} for different sea state conditions. This is shown in Fig.16 below and includes a best-fit curve for the observed trend. Also shown in this figure are our corresponding model results based on our computed $S_{ds}^{loc}(c)$ and $\Lambda(c)$ results, as reported in Zappa et al. (2016). The corresponding model results of Sutherland and Melville (2015) are also shown.

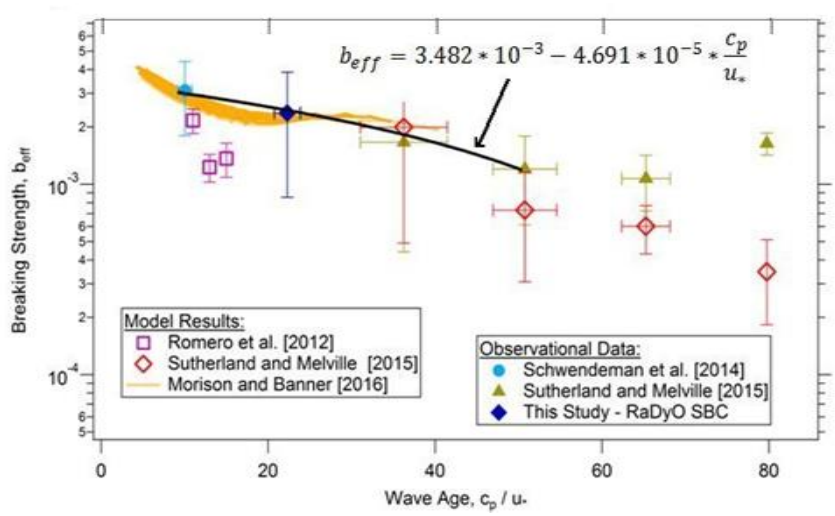

Figure 16. Variation of the measured mean spectral breaking strength b_{eff} with the wave age of the wind sea. The data sets used are shown in the right hand legend. The modeled results are shown in the left hand legend, including our results. The solid black curve is an optimal parametric fit [from Zappa et al., 2016].

4.5 Benchmark E - Overall consistency between wind input and dissipation rates

Driving the transition from growing to mature seas is the source term balance, shown below in Fig.17, for both moderate winds (6 m/s) and strong (24 m/s). A most interesting feature is that even though the wind input to the dominant waves decreases to well below the dissipation rate as the wave speed approaches the wind speed, the dominant wave saturation level (and steepness) remains sufficiently large for the breaking to occur through nonlinear wave group interactions (see Banner and Peirson (2007)).

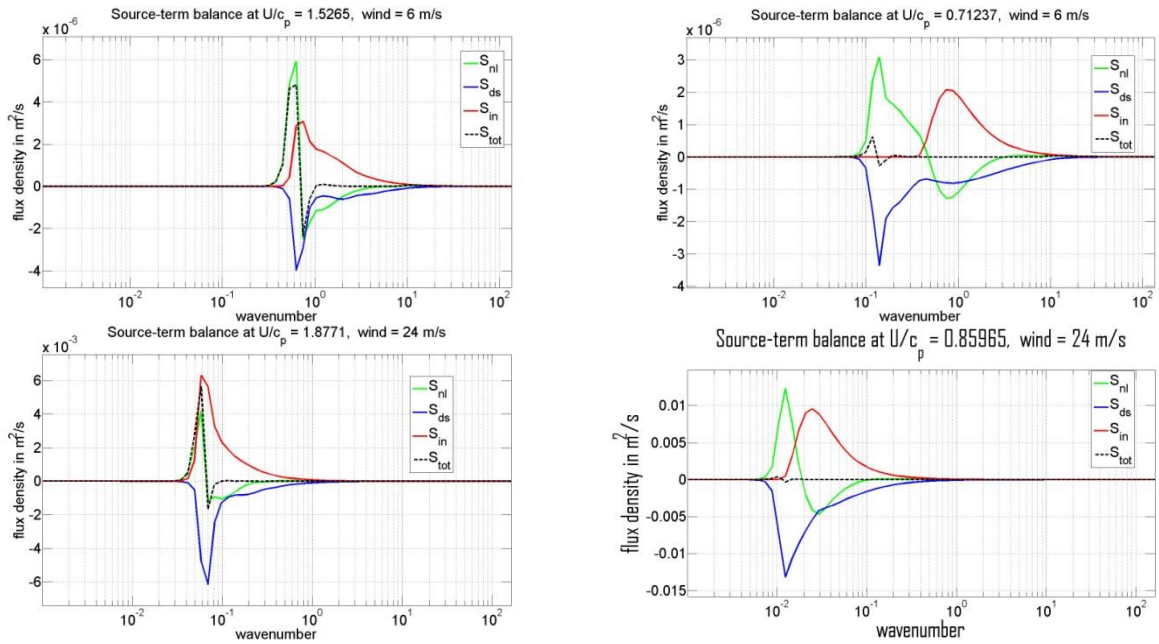

Figure 17. Source term balance for U_{10} = 6 m/s (upper panels) and 24 m/s (lower panels) for young (left panels) and maturing (right panels) seas.

Our proposed form (2) for S_{ds} is able to account for breaking onset and loss rates during the transition to swell. This situation arises for maturing wind seas, where the wind input to these longest waves is greatly reduced. At this stage of evolution for the 6 m/s wind speed case, the dominant balance is between the dissipation and nonlinear transfer (see the upper right panel in Fig.17 upper panels), where the dissipation is primarily background turbulence as the spectral peak saturation level falls below the breaking threshold.

We verified that during the evolution at each wind speed, the integrated wind input and dissipation rates closely tracked each other, with the dissipation rate approaching the wind input rate as the seas age. The integrated nonlinear transfer term was zero at each timestep. Given that the total wind input to the waves is less than the total wind input to the sea surface, and that the drag coefficients are realistic, the modeled dissipation rates appear to be very plausible.

Our wind input and dissipation rate source term behavior with wave age showed interesting properties when reviewed over a wide range of wind speeds. These are conveniently plotted in a normalized form in Fig.18 using $u_*^2 c_p$ to collapse the very large dynamic range with wind speed, where c_p is the spectral peak phase speed.

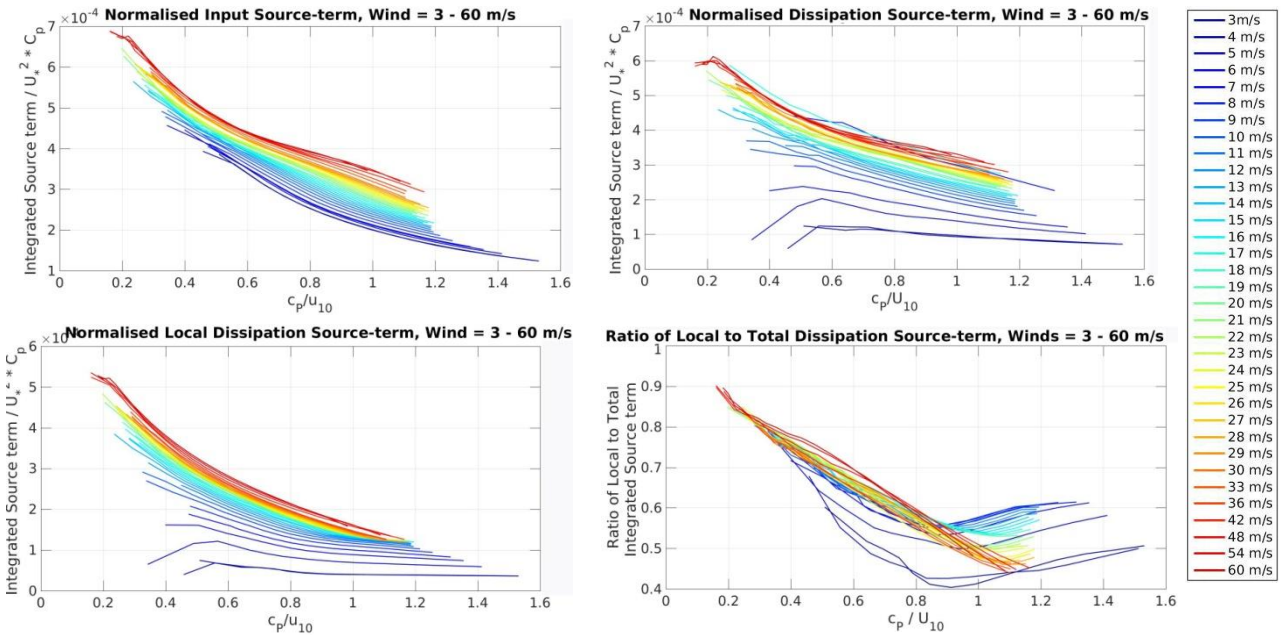

Figure 18. Integrated source terms normalized by $u_*^2 c_p$ (upper left) wind input energy flux (upper right) dissipation rate (lower left) local dissipation rate (lower right) ratio of local to total dissipation rate.

Fig.18 shows the source terms and their components, normalised by $u_*^2 c_p$. Even though the source terms vary over four or more orders of magnitude, their normalised integrals come close to falling onto single curves. The non-local components of the dissipation rate do not normalize as well as the input or local dissipation rate, hence the total dissipation and the fraction of the local-to-total dissipation rate show a greater spread.

Fig.19 below shows the behavior of the evolution of the integrated source terms as the seas age at four different wind speeds. It is seen that the integrated S_{in} and S_{ds} terms initially increase then decrease towards large wave age. They asymptote towards each other as the wind sea matures, although the input is always greater than the dissipation. This suggests that the wind sea will continue to grow, but at an ever-decreasing rate. The integrated S_{nl} term is zero for all times, as required. In addition to the overall wind input momentum flux, as expressed by the drag coefficient (see Fig.9 in section 4.3 above), another important validation check can be made using the total wave energy dissipation rate in the water column, reflected in the integrated dissipation rate S_{ds}.

For wave age around $c_p/U_{10} \sim 1.2$, the winds and dominant waves are largely decoupled energetically, and the total dissipation rate S_{ds} in the wave evolution equation mirrors the total dissipation rate in the wave boundary layer, which has been investigated observationally in considerable detail in recent measurements (Sutherland and Melville, 2015, Fig.16). This has allowed a valuable assessment of the validity of our S_{ds} model formulation results, which correspond closely to the observations for the available cases.

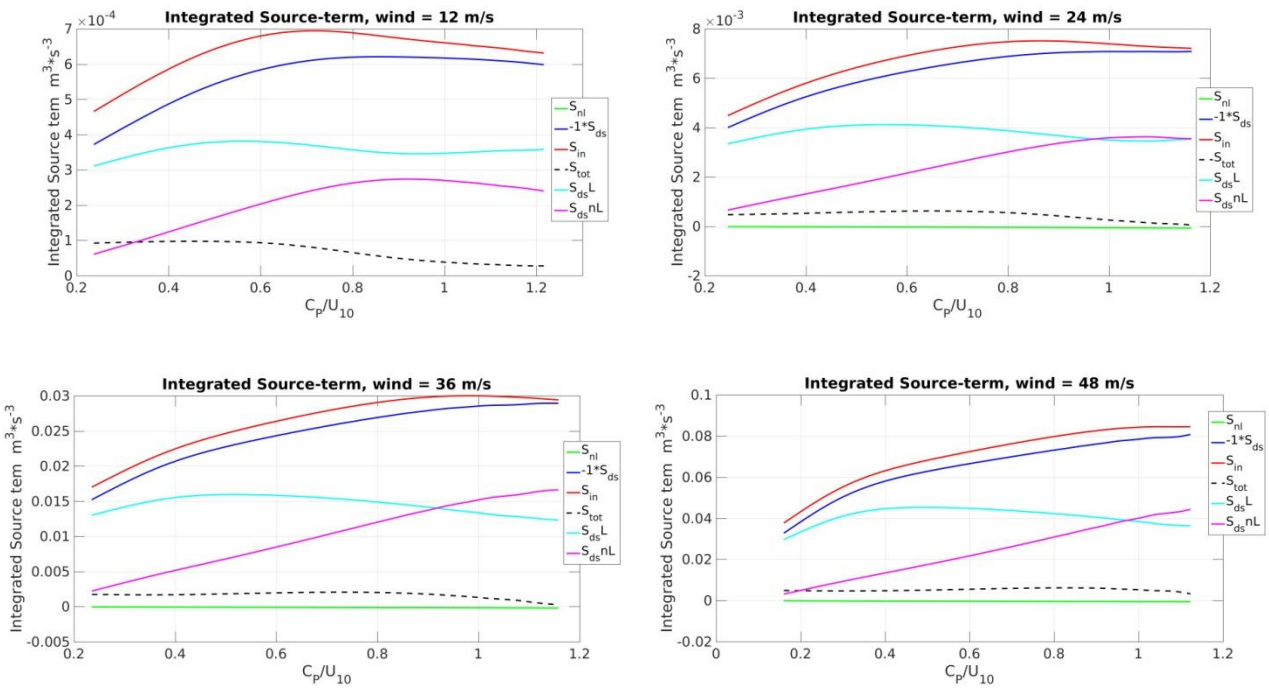

Figure 19. Evolution of the integrated source terms as the seas age, for wind speeds of 12, 24, 36 and 48 m/s.

4.6 Wave model performance - Case study of very young wind sea evolution

We investigated the performance of our refined source terms for wave dissipation and wind input integrated over the spectrum against the observed terms during the young wind sea growth episode in the Strait of Juan de Fuca reported by Schwendeman et al. (2014). The results in Fig. 20 compare the fetch evolution of our modeled integrated S_{in} and S_{ds} source terms with those observed (left panel) and the computed versus observed significant wave height H_s (right panel). The close correspondence of the results is very reassuring.

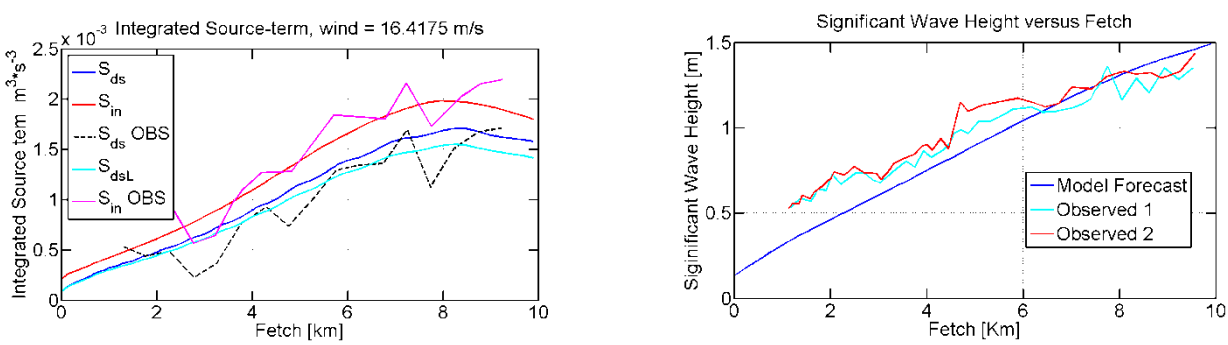

Figure 20. Comparisons of modeled and observed fetch evolution of the source terms for the Strait of Juan de Fuca experiment. Left panel shows the spectrally-integrated modeled wind input S_{in} (red), observed total input (magenta), computed total dissipation rate S_{ds} (blue), which is dominated by the wave breaking component S_{ds}^{loc} (cyan), and the observed dissipation rate (black dashed line). The right panel shows the modeled significant wave height H_s (blue) versus the two available observations (cyan, red).

4.7 Summary of wave model results

In this study, a framework for incorporating wave breaking predictions of breaking crest length density and strength of the dominant wind waves into sea state forecast models has been developed. It has been validated under the assumption that it will be implemented in conjunction with the exact form of the nonlinear spectral transfer term S_{nl}, together with a suitable wind input source term formulation S_{in}. Because of the computational cost, our validations have been limited to idealized cases, particularly duration-limited, unidirectional (but possibly non-stationary) winds. These cases provided a cost-effective but limited validation regime and further validation is needed. This is presently underway, as described in section 4.10 below. Validation of breaking wave forecasts at very high wind speeds is clearly needed, but is presently hampered by the lack of observational breaking data for severe wind speeds.

Overall, the model framework we have developed and refined in this study has performed very well over a particularly wide range of wind speeds according to the five benchmarks designed to provide a critical testbed of the model's capabilities. The outcome is that the model is in principle ready for implementation into an operational prototype, as recommended in section 4.10 below.

4.8 Sea spray forecasts

As an additional output from the wave model, we developed a unified air-sea flux parameterization that incorporates winds, waves and sea spray generation.

We developed a parameterization structure for the estimation of the fluxes of momentum, sensible heat, and latent heat over the ocean. The parameterization is principally intended for use in coupled air-ocean-wave models. It is based on a combination of the NOAA COARE bulk flux parameterization and the Fairall-Banner-Morison (FBM) sea spray parameterization. COARE3.5 is the latest version (Edson et al., 2013). It has been fitted to 15,000 hrs of direct covariance flux data for wind speeds from 0 – 25 m/s. The original FBM model (documented in Fairall et al., 2009) is a scaling model where sea spray is produced by breaking waves. Droplet production is driven by energy dissipated by wave breaking. Ejection into the atmospheric flow is scaled by wind speed, slope of the dominant wave. Droplet evaporation physics are used to compute the effects of the spray on the total (direct and spray-mediated) heat and moisture fluxes. The COARE and FBM models have been upgraded based on the idealized wave model calculations using the UNSW wave model described above. The wind stress in the COARE data and the wave model are well-described by a Charnock parameter, α, of the form $\alpha = A(u_* / c_p)^B$.

The FBM model has been extended to allow use of the spectral version S_{ds} (**k**) of the wave breaking dissipation rate source term. Thus the spray production by each wavenumber of the breaking spectrum is computed and the total spray production is the sum over the spectrum. Three versions of the code have been developed - fully physical, partially parameterized and fully parameterized – depending on the data available from the parent coupled model.

Examples of the model output of heat fluxes for hurricane surface layer conditions (SST=29° C, air T=27° C, and RH=90%) at 24 m/s and 48 m/s are shown in Fig.21. The use of spectrally-resolved droplet production has a significant effect on droplet production in this model. Earlier versions of the model assumed all droplets were produced by the total wave dissipation from the dominant wave breaking. The spectral version produces droplets at each wave phase speed proportional to the dissipation rate associated with those waves; total production is then

computed as the integral over the spectrum. The result is a relatively large increase in the droplet mass flux from younger waves (see Fig.21). We currently maintain codes of the model at three different levels of computation.

1.0 Fully physical: Here all of the inputs to the droplet algorithm come completely from elsewhere (observations, coupled atmosphere wave model). The inputs are used to compute the drop spectrum, the spectrum is used in the thermodynamic time scale code to compute the drop sensible and latent heat values, and the feedback code computes the final values.

2.0 Partly parameterized: Here fluxes are initially computed via a bulk flux algorithm to obtain u_*. Wave properties (C_{wave}, h_{wave}, and P) are computed using mathematic fits from a wave model (e.g., the UMiami, URI or the UNSW models). The drop heat and moisture fluxes are explicitly computed; feedback is computed.

3.0 Fully parameterized: Here the basic bulk flux and wave property inputs are computed from parameterizations as in case 2. However, the thermodynamics are also calculated via a parameterization. Again, feedback is computed. This approach uses the least code and is the most parameterized.

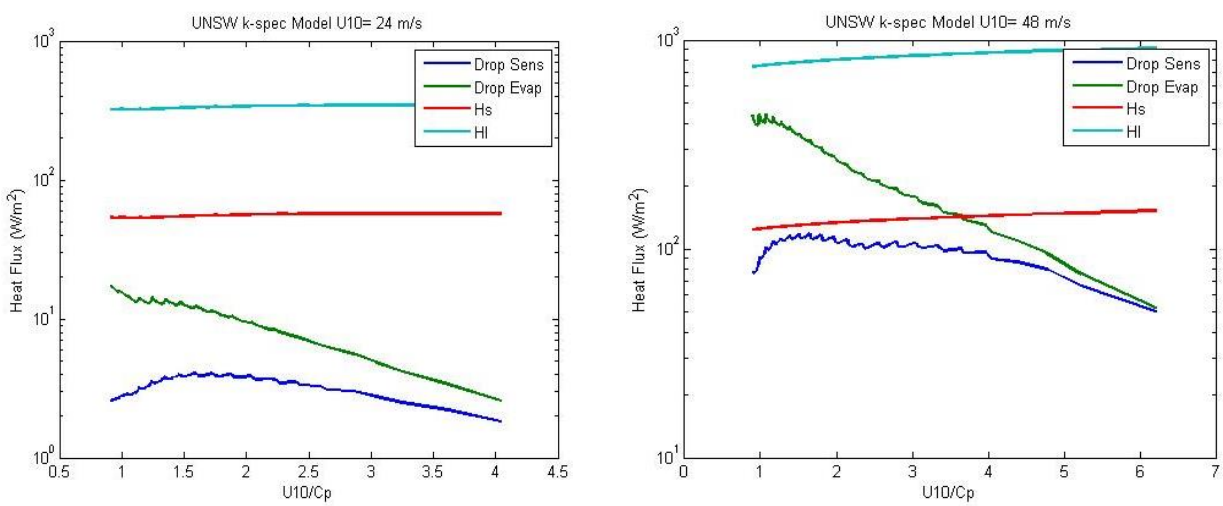

Figure 21. Example model calculations of sensible and latent heat flux at the surface using the UNSW wave model output at U_{10}=24 m/s (left panel) and U_{10}=48 m/s (right panel). The red and cyan lines are the normal direct transfers of sensible and latent heat. The blue and green lines are the droplet contributions.

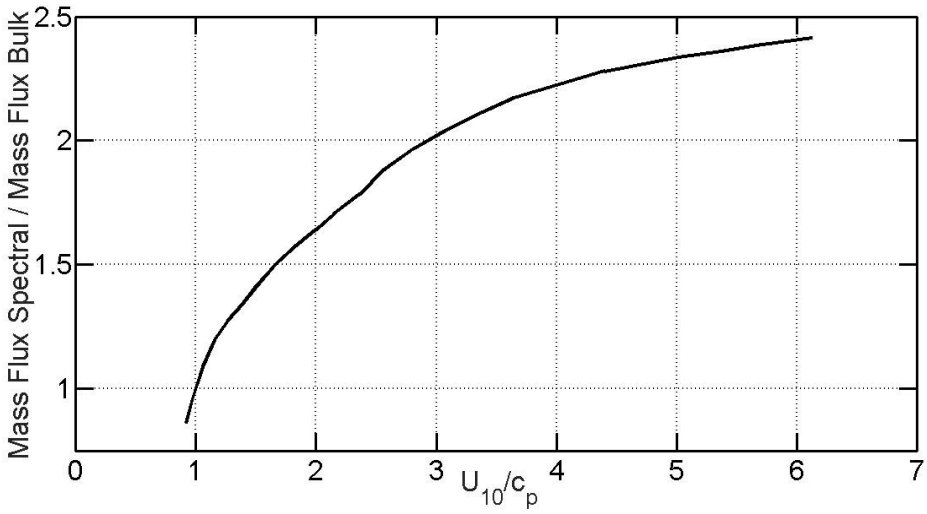

Figure 22. Ratio of the sea spray mass flux from our sea state dependent model to that from a standard windspeed-only model plotted against the inverse wave age (U_{10}/c_p). Note how the ratio of the mass flux changes as the inverse wave age increases from old seas (left side) where breaking at the spectral peak is minimal, towards very young seas (right side) where there is frequent breaking of the spectral peak waves. The results shown are for U_{10}=24 m/s.

4.9 Full coupling of the wave model to the wind field

With the very encouraging validation to date of our 'semi-coupled' framework, it is feasible to transition it to a fully coupled version. This would require a full atmospheric model, using a suitable wind input growth rate parameterization that ideally would depend on a scale-dependent wind velocity, such as $U(\lambda/2)$, where λ is the water wavelength. This is presently ongoing through a collaborative effort with NCEP Marine Modeling and Analysis Branch.

4.10 Transition to operations

The breaking wave model framework developed in this project has been built around the 'Exact' NL source term for S_{nl}, as we sought to choose the most accurate source terms, albeit at the cost of computational speed. However, the approximate form of S_{nl} in widespread operational use, known as the Direct Interaction Approximation (DIA), at each timestep computes only one of the wave-wave resonance interaction terms of the millions that are computed by the 'Exact' NL source term. Needless to say, the results can be very different, and we wanted to eliminate this from our model development.

A much closer approximation known as the Two-Scale Approximation (TSA) has been developed recently (Resio and Perrie, 2008). Its performance appears to match the Exact NL very closely and hence may be a suitable replacement for Exact NL in operations. This is an exciting and timely development that needs careful examination.

4.11 Highlights of the SPANDEX study

SPANDEX, the Spray Production and Dynamics Experiment, is a laboratory study conducted at the UNSW Water Research Laboratory in Manly Vale, Sydney, Australia. The goals of

SPANDEX were to illuminate physical aspects of spume droplet production and dispersion, verify theoretical simplifications presently used to estimate the source function from ambient droplet concentration measurements, and examine the relationship between the implied source strength and forcing parameters such as wind speed, surface turbulent stress, and wave properties. Our observations of droplet profiles give reasonable confirmation of the basic power-law profile relationship that is commonly used to relate droplet concentrations to the surface source strength. This essentially confirms that, even in a wind tunnel, there is a near balance between droplet production and removal by gravitational settling. Phase Doppler Anemometry observations revealed significant mean horizontal and vertical slip velocities that were larger closer to the surface. The magnitude seems too large to be an acceleration time scale effect, so we hypothesize that the droplets tend to be found in vertically moving air masses (e.g., updrafts departing from wave crests). Scaling of the droplet production surface source strength proved to be difficult to explain quantitatively. The wind speed forcing varied only 23% and the stress increased by a factor of 2.2. Yet, the source strength increased by about a factor of 10. We attempted to relate this to an estimate of surface wave energy flux through calculation of the standard deviation of small-scale surface disturbance combined with wind forcing. This energy flux index only increased 52% with the wind forcing, so it is not clear that we have characterized energy flux correctly. Nonetheless, a graph of spray mass surface flux versus surface disturbance energy is quasi-linear with a substantial threshold.

Laboratory Study of Sea Spray from Breaking Waves: Part I - Profiles of Droplet Microphysical Properties
C.W. Fairall, C.J. Zappa, S. Brumer, M.L. Banner, R.P. Morison, X. Yan and W.L Peirson.

This laboratory study was performed to develop an accurate sea spray source function parameterization through coincident observations of sea spray along with wave breaking, turbulent kinetic energy dissipation rate and turbulent fluxes. It continued the Spray Production and Dynamics Experiment (SPANDEX) conducted at the UNSW Water Research Laboratory in Manly Vale (NSW, Australia). SPANDEX I is described in Fairall et al. (2009). SPANDEX II was carried out during June 2010 and featured several observational advances compared to SPANDEX I: direct measurements of ocean-side turbulence profiles and thermal imaging of individual spray drops. Spray drops were measured with an optical array size spectrometer. Properties of the sea spray profiles as a function of forcing were measured and compared to a theoretical profile based on balancing turbulent upward transport and gravitational settling.

A Laboratory Study of Sea Spray from Breaking Waves. Part II – Correlations with Wind and Wave Properties. C.J. Zappa, M.L. Banner, C.W. Fairall, D. LeBel, S. Brumer, R.P. Morison, X. Yan and W.L. Peirson.

Field measurements of spray flux show significant variability based on wind speed or friction velocity. The process of spray flux is linked fundamentally to wave breaking, as well as wind speed. In SPANDEX I, the laboratory experiments used surrogates for dissipation due to breaking. In SPANDEX II, we performed the first study investigating spray flux dependence on water-side dissipation rate, rather than wind speed. From our laboratory wind wave tank study with salt water (30 psu) we found that correlating with u_*^3 showed a near-linear dependence. Correlating with the integrated dissipation rate also showed a near-linear dependence. If these encouraging initial results is followed up in a field study and reveal a robust correlation of spray

flux with the integrated dissipation rate, it could be possible to estimate sea spray flux reliably from the dissipation rate estimated from a wave model.

4.12 Benefits Analysis Summary

4.12.1 Technical Output

During the course of this project, several refereed publications have been published in leading journals, with several in preparation, as well as a number of conference and workshop contributions.

Refereed papers published

C.J. Zappa, M.L. Banner, R.P. Morison and S.E. Brumer, 2016: On the variation of the effective breaking strength in oceanic sea states. *J. Phys. Oceanogr.* doi: http://dx.doi.org/10.1175/JPO-D-15-0227.1

M.L. Banner, X. Barthelemy, F. Fedele, M. Allis, A. Benetazzo, F. Dias and W.L. Peirson, 2014: Linking reduced breaking crest speeds to unsteady nonlinear water wave group behavior. *Phys. Rev. Lett. 112, 114502.*

M.L. Banner, C. J. Zappa, & J. Gemmrich, 2014: A Note on Phillips' Spectral Framework for Ocean Whitecaps, *J. Phys. Oceanography*, 44, 1727-1734.

Peirson, W.L., J.W. Walker and M.L. Banner, 2014: On the microphysical behaviour of wind-forced water surfaces and consequent re-aeration. *J. Fluid Mech. 743, 399-447.*

Tolman, H.L., M.L. Banner & J.M. Kaihatu, 2013. The NOPP operational wave model improvement project. Ocean Modelling, 70, 2-10. http://dx.doi.org/10.1016/j.ocemod.2012.11.011

J.R. Gemmrich, C.J. Zappa, M.L Banner and R.P. Morison, 2013. Wave breaking in developing and mature seas**.** *J. Geophys. Res. Oceans*, 241, 118, 4542 – 4552, doi: 10.1002/jgrc.20334.

Zappa, C. J., M. L. Banner, H. Schultz, J. R. Gemmrich, R. P. Morison, D. A. LeBel, and T. Dickey (2012): An overview of sea state conditions and air-sea fluxes during RaDyO. J. Geophys. Res., 117, C00H19, doi:10.1029/2011JC007336.

Banner, M.L. and R.P. Morison, 2010: Refined source terms in wind wave models with explicit wave breaking prediction. Part I: Model framework and validation against field data. Ocean Modell. doi:10.1016/j.ocemod.2010.01.002.

Refereed papers submitted

X. Barthelemy, M.L. Banner, W.L. Peirson, F. Dias and M. Allis, 2015: On the local properties of highly nonlinear unsteady gravity water waves. Part 1. Slowdown, kinematics and energetics. Submitted to J. Fluid Mech. (pdf available at *arXiv:1508.06001*)

X. Barthelemy, M.L. Banner, W.L. Peirson, F. Fedele, M. Allis, F. Dias, 2015: On the local properties of highly nonlinear unsteady gravity water waves. Part 2. Dynamics and onset of breaking. Submitted to J. Fluid Mech. (pdf available at *arXiv:1508.06002*)

A. Saket, W.L. Peirson, M.L. Banner, X. Barthelemy and M. Allis, 2015: Wave breaking onset of two-dimensional deep-water wave groups in the presence and absence of wind. Submitted to J. Fluid Mech. (pdf available at *arXiv:1508.07702* **).**

M.L. Banner and R.P. Morison, 2016: On the upper ocean turbulent dissipation rate due to very short breaking wind-waves. Submitted to Ocean Modelling. (pdf available at *arXiv:1602.06649*).

Refereed journal papers in preparation, to be submitted

R.P. Morison & M.L. Banner, 2016: Forecasting wave breaking in ocean wind wave models. Part II. Model performance over a wide wind speed range.

C.W. Fairall, M.L. Banner, W.L. Peirson and R.P. Morison, 2016: Wave breaking and turbulence model of spume droplet production: a physically-based parameterization of the sea-spray large droplet source function.

C.W. Fairall, M.L. Banner and R.P. Morison, 2016: A unified air-sea flux parameterization incorporating winds, waves and sea spray generation.

C. J. Zappa, C.W. Fairall, M.L. Banner, W.L. Peirson, D. LeBel and R.P. Morison, 2016: A laboratory study of wind-driven sea spray from breaking waves.

Conference Research seminars presented

R.P. Morison and M.L. Banner, Progress on Dangerous Breaking Wave Warnings from Spectral Wave Forecast Models. 14th International Workshop on Wave Hindcasting and Forecasting, and 5th Coastal Hazards Symposium, Key West, Florida, USA, Nov 8-13, 2015.

M.L. Banner, X. Barthelemy, F. Fedele, M. Allis, A. Benetazzo, F. Dias, W.L. Peirson. Linking reduced breaking crest speeds to unsteady nonlinear water wave group behavior. Waves in Shallow Water Environments (WISE) workshop, 8-12 June 2014, ECMWF, Reading, U.K.

R.P. Morison and M.L. Banner. Incorporating Breaking Wave Predictions in Spectral Wave Forecast Models. 13th International Workshop on Wave Hindcasting and Forecasting & 4th Coastal Hazards Symposium, Oct. 27- Nov.1 2013, Banff, Canada.

Fairall, C.W., C.J. Zappa, S. Brumer, M.L. Banner, R.P. Morison, X. Yan and W.L Peirson, 2012: Laboratory study of sea spray from breaking waves: Part 1 - Profiles of droplet microphysical properties. 18th AMS Conference on Air-Sea Interaction, Boston, 8-13 July, 2012

R.P. Morison, M.L. Banner, H.J. Alves, P.P. Sullivan. Wind Wave Model Performance in Relaxing Wind Seas. 12th International Workshop on Wave Hindcasting and Forecasting & 3rd Coastal Hazard Symposium, Oct.30 – Nov. 4, 2011, Kohala Coast, Hawaii.

4.12.2 Strategic Implications

Negotiations are underway with NCEP/Marine Modeling and Analysis Branch, NOAA to investigate transitioning this modeling framework for forecasting wave breaking properties of interest into WaveWatch III for expanding the range of forecast products to enhance public warnings of dangerous breaking wave conditions.

Acknowledgements

The authors gratefully acknowledge the support from ONR during the course of this study. We also benefited from technical discussions with our colleagues Peter Sullivan at NCAR and interactions with colleagues Christopher Zappa at Columbia University, Francesco Fedele at Georgia Tech and William Peirson at the University of New South Wales, Australia.

References

Alves, J.H and M.L. Banner, 2003: Performance of a saturation-based dissipation source term for wind wave spectral modelling, *J. Phys. Oceanogr*. 33, 1274-1298.
Ardhuin, F., B. Chapron, and F. Collard, 2009: Observation of swell dissipation across oceans, *Geophys. Res. Lett*., 36, L06607, doi:10.1029/2008GL037030.
Alves, J.H and M.L. Banner, 2003: Performance of a saturation-based dissipation source term for wind wave spectral modelling, *J. Phys. Oceanogr*. 33, 1274-1298.
Ardhuin, F., B. Chapron, and F. Collard, 2009: Observation of swell dissipation across oceans, *Geophys. Res. Lett*., 36, L06607, doi:10.1029/2008GL037030.
Banner, M.L., I.S.F Jones and J.C. Trinder, 1989: Wavenumber spectra of short gravity waves. *J. Fluid Mech.* 198, 321-344.
Banner, M.L., 1990a: The influence of wave breaking on the surface pressure distribution in wind wave interactions. *J. Fluid Mech.* 211, 465-493.
Banner, M.L., 1990b: Equilibrium spectra of wind waves. *J. Phys. Oceanogr*., 20, 966-984.
Banner, M.L. and Peregrine, D.H., 1993: Wave breaking in deep water. *Ann. Rev. Fluid Mech.*, 25, 373-397
Banner, M.L. and W.L. Peirson, 1998: Tangential stress beneath wind-driven air-water interfaces. *J. Fluid Mech.* 364, 115-145.
Banner, M.L., Babanin, A.V., Young, I.R., 2000: Breaking probability for dominant waves on the sea surface. *J. Phys. Oceanogr*. 30, 3145–3160.
Banner, M.L., J.R. Gemmrich and D.M. Farmer, 2002: Multiscale measurements of ocean wave breaking probability. *J. Phys. Oceanogr*. 32, 3364-3375.
Banner, M.L. & W.L. Peirson, 2007: Wave breaking onset and strength for two-dimensional deep water wave groups. *J. Fluid Mech.*, 585, 93-115.
Banner, M.L. and R.P. Morison, 2010 Refined source terms in wind wave models with explicit wave breaking prediction. Part I: Model framework and validation against field data. *Ocean Modell*. doi:10.1016/j.ocemod.2010.01.002.
Donelan, M.A., A.V. Babanin, I.R.Young and M.L. Banner, 2006: Wave follower field measurements of the wind input spectral function. Part II. Parameterization of the wind input. J. Phys. Oceanogr., 36, 1672-1688.
Drazen, D. A., Melville, W. K. & Lenain, L. 2008 Inertial estimates of dissipation in unsteady breaking waves. J. Fluid Mech. 611, 307u
Edson, J.B., J. V. S. Raju, R.A. Weller, S. Bigorre, A. Plueddemann, C.W. Fairall, S. Miller, L. Mahrt, Dean Vickers, and Hans Hersbach, 2013: On the Exchange of momentum over the open ocean. *J. Phys. Oceanogr.*, 43, 1589–1610. doi: http://dx.doi.org/10.1175/JPO-D-12-0173.1
Fairall, C.W., C.J. Zappa, S. Brumer, M.L. Banner, R.P. Morison, X. Yan and W.L Peirson, 2012: Laboratory study of sea spray from breaking waves: Part 1 - Profiles of droplet microphysical properties. 18th AMS Conference on Air-Sea Interaction, Boston, 8-13 July, 2012
Fairall, C.W., M.L. Banner, W.L. Peirson, W. Asher and R.P. Morison, 2009: Investigation of the physical scaling of sea spray spume droplet production. J. Geophys. Res. 114, C10001, doi:10.1029/2008JC004918.
Gemmrich, J. R. and D. M. Farmer, 1999: Observations of the scale and occurrence of breaking surface waves. *J. Phys. Oceanogr.*, 29, 2595–2606.
Gemmrich, J. R. & Farmer, D.M., 2004: Near-surface turbulence in the presence of breaking waves. *J. Phys. Oceanogr*, 34, 1067-1086.
Gemmrich, J. R., C.J. Zappa, M.L. Banner, and R.P. Morison, 2013: Wave breaking in developing and mature seas. *J. Geophys. Res.- Oceans*, 118, 4542–4552.
doi: 4510.1002/jgrc.20334.
Hasselmann, K., 1962: On the non-linear energy transfer in a gravity-wave spectrum Part 1. General theory. Journal of Fluid Mechanics, 12, pp 481-500 doi:10.1017/S0022112062000373

Hsiao, S.V., and O.H. Shemdin, 1983: Measurements of wind velocity and pressure with a wave follower during MARSEN. *J. Geophys. Res*., 88, 9841-9849.
Hwang, P.A. and D.W. Wang, 2004: Field measurements of duration-limited growth of wind-generated ocean surface waves at young stage of development. *J. Phys. Oceanogr.*, 34, 2316-2326.
Janssen, P.A.E.M., 1991: Quasi-linear theory of wind-wave generation applied to wave forecasting. *J. Phys. Oceanogr.*, 21, 1631-1642.
Kleiss, J. M. and W. K. Melville, 2010: Observations of wave breaking kinematics in fetch-limited seas. *J. Phys. Oceanogr.*, 40, 2575-2604.
Komen, G.J., L. Cavaleri, M.A. Donelan, K. Hasselmann, S. Hasselmann & P.A.E.M. Janssen, 1994: Dynamics and Modelling of Ocean Waves, Cambridge University Press, Cambridge, 532pp.
Kukulka, T., and H. Hara, 2008a: The effect of breaking waves on a coupled model of wind and ocean surface waves. Part I: Mature seas. *J. Phys. Oceanogr.*, 38**,** 2145–2163.
Kukulka, T., and H. Hara, 2008b: The effect of breaking waves on a coupled model of wind and ocean surface waves. Part II. Growing seas. *J. Phys. Oceanogr.*, 38**,** 2164–2184
Melville, W.K., 1996: The role of surface-wave breaking in air-sea interaction. *Ann. Rev. Fluid Mech*, **26**, 279-321
Miles, J.W., 1957: On the generation of surface waves by shear flows. *J. Fluid Mech.*, 3, 185-204.
R.P. Morison & M.L. Banner, 2016: Forecasting wave breaking in ocean wind wave models. Part II. Model performance over a wide wind speed range. To be submitted.
Perlin, M., W. Choi and Z. Tian, 2013: Breaking waves in deep and intermediate waters. Annu. Rev. Fluid Mech., 45, 115–145, doi:10.1146/annurev-fluid-011212-140721.
Phillips, O.M., 1985: Spectral and statistical properties of the equilibrium range in wind-generated gravity waves. *J. Fluid Mech.*, 156, 505-531.
Plant, W.J., 1982: A relation between wind stress and wave slope. *J. Geophys. Res.* 87, 1961-1967.
Resio, D., and Perrie, W. A., 2008: Two-scale approximation for efficient representation of nonlinear energy transfers in a wind wave spectrum. Part 1: Theoretical Development. J. Phys. Oceanogr., 38, 2801-2816.
Romero, L. and W.K. Melville, 2010: Airborne observations of fetch-limited waves in the Gulf of Tehuantepec. J. Phys. Oceanogr., 40, 441-465.
Romero, L., W.K. Melville, and J. Kleiss, 2012: Spectral energy dissipation due to surface-wave breaking. *J. Phys. Oceanogr.***,** doi:10.1175/JPO-D-1111-1072.1171.
Schwendeman, M., J. Thomson, and J.R. Gemmrich, 2014: Wave breaking and dissipation in a young wind sea. *J. Phys. Oceanogr* , 44, 10-127. DOI 10.1002/2015JC011196
Song, J. and M. L. Banner, 2002: On determining the onset and strength of breaking for deep water waves. Part 1: Unforced irrotational wave groups. *J. Phys. Oceanogr*. 32, 2541-2558.
Snyder, R.L, F.W. Dobson, J.A. Elliott, and R.B. Long, 1981 : Array measurements of atmospheric pressure fluctuations above surface gravity waves. *J. Fluid Mech.* 102, 1-59.
Sullivan, P.P., and J.C. McWilliams, 2010: Dynamics of winds and currents coupled to surface waves. *Annu. Rev. Fluid Mech.*, 42**,** 19-42.
Sutherland, P., and W.K. Melville, 2013: Field measurements and scaling of ocean surface wave-breaking statistics. *Geophys. Res Lett.*, 40**,** 3074–3079.
Sutherland, P., and W.K. Melville, 2015: Field measurements of surface and near-surface turbulence in the presence of breaking waves. *J. Phys. Oceanogr.*, 45, 943-965.
Terray, E.A., M.A. Donelan, Y.C. Agrawal, W.M. Drennan, K.K. Kahma, A.J. Williams III, P.A. Hwang, and S.A. Kitaigorodskii, 1996: Estimates of kinetic energy dissipation under breaking waves. *J. Phys. Oceanogr*., 26, 792-807
Tian Z, M. Perlin, M., W. Choi, 2010: Energy dissipation in two-dimensional unsteady plunging breakers and an eddy viscosity model. *J. Fluid Mech.* 655:217–57
Tolman, H.L., M.L. Banner & J.M. Kaihatu, 2013. The NOPP operational wave model improve-ment project. Ocean Modelling, 70, 2-10. http://dx.doi.org/10.1016/j.ocemod.2012.11.011
Tracy, B.A. and D.T. Resio, 1982: Theory and calculation of the nonlinear energy transfer between sea waves in deep water, WIS Rept 11, US Army Engineers Waterway Experiment Station.

Yang, M., B.W. Blomquist, and P. D. Nightingale, 2014: Air-sea exchange of methanol and acetone during HiWinGS: Estimation of air phase, water phase gas transfer velocities, J. Geophys. Res., Oceans, 119, 7308–7323, doi:10.1002/2014JC010227.
Young, I.R., 1999: Wind generated ocean waves. Elsevier, 288 pp.
Zappa, C.J., M.L. Banner, R.P. Morison and S.E. Brumer, 2016: On the variation of the effective breaking strength in oceanic sea states. *J. Phys. Oceanogr*. doi: http://dx.doi.org/10.1175/JPO-D-15-0227.1